NASA TN D-1024

NASA TN D-1024

TECHNICAL NOTE

D-1024

MEASURED SURFACE DEFECTS ON TYPICAL TRANSONIC AIRPLANES AND ANALYSIS OF THEIR DRAG CONTRIBUTION

By Elmer A. Horton and Neal Tetervin

Langley Research Center
Langley Station, Hampton, Va.

CASE FILE COPY

NATIONAL AERONAUTICS AND SPACE ADMINISTRATION

WASHINGTON October 1962

NATIONAL AERONAUTICS AND SPACE ADMINISTRATION

TECHNICAL NOTE D-1024

MEASURED SURFACE DEFECTS ON TYPICAL TRANSONIC AIRPLANES AND ANALYSIS OF THEIR DRAG CONTRIBUTION

By Elmer A. Horton and Neal Tetervin

SUMMARY

Quantitative measurements are presented of the surface defects existing on three different operational airplanes. Estimates of the drag increments associated with each type of surface irregularity and comparisons of drags measured on models and the full-scale aircraft indicate that the total drag contribution of the defects is an important percentage of the total airplane drag.

INTRODUCTION

The problem of predicting full-scale flight drag from wind-tunnel model tests has been beset with a great deal of confusion over the years. One approach to the problem has been to collect flight drag data for a number of aircraft and to compare these data with wind-tunnel drag data for models of these aircraft. This comparison would presumably supply empirical corrections. Unfortunately, however, flight drag data are not only difficult to obtain with sufficient accuracy for this purpose but the actual flight configuration usually differs significantly from the model configuration with the result that data available for establishing such an empirical criterion are extremely limited.

A much more direct and rational approach used in recent years involves the use of the basic skin-friction laws which are well-known and firmly established over a wide range of Reynolds number and Mach number. In this procedure, model tests are made with transition fixed near the component leading edges and the model skin-friction drag is first reduced by the decrease in turbulent skin friction of a flat plate over the Reynolds number range from model to flight conditions. This step in the procedure has been justified by tests such as those of reference 1 which shows excellent agreement in the drag results from tunnel and rocket-propelled tests of a complete airplane configuration at widely different Reynolds number when the tunnel drag data are extrapolated to the flight Reynolds number. Next, if the aircraft designer feels confident, after a realistic appraisal of the situation, that certain areas

of the aircraft have laminar rather than turbulent flow, he would be justified in reducing the extrapolated drag to allow for this effect. Finally, an allowance must be included for drag-producing elements such as rivets, butt joints, gaps, and surface scratches that are present on the actual airplane but not simulated on the model.

The purpose of this paper is to provide a quantitative measure of the surface defects existing on actual operational airplanes and an indication of the drag contribution of these defects.

SYMBOLS

A wing area (plan view)

a slope of "least squares" straight line

B "least squares" constant for slot data

b slope of straight line

C ratio of projected area on plate of one surface distortion (grain of sand) to the product wL

C_1 projected area of all surface distortions (grains of sand) per unit area of surface

$C_2 = \frac{h}{w}\frac{C_1}{C}$

C_D drag coefficient based on wing planform area

$C_{D,f}$ skin-friction drag coefficient

C_f compressible friction coefficient

C_{f_i} incompressible friction coefficient

$C_{D,s}$ drag coefficient of slot or scratch, $\frac{D_s}{\frac{\rho}{2} U^2 w}$

ΔC_D incremental drag coefficient obtained by extrapolating from model to full-scale Reynolds number

D_s	drag of slot or scratch per unit length of slot or scratch
E	sum of squares of errors
$F(\ )$	function of $f(\ )$ for sand grains
$f(\ )$	function of $\frac{hv_0}{\nu_0}$
$f_r(\ )$	function of $\frac{hv^*}{\nu}$
f_s	function of $\frac{hv^*}{\nu}$ for slots
f_1	function of $\log_{10} \frac{hv^*}{\nu}$
h	height of grain of sand or depth of slot or scratch
K	constant in Sutherland's formula
L	length of projection or depression in a direction perpendicular to stream
L_s	length of slot or scratch
M	Mach number
N	number of projections per unit area
n	number of projections on surface of area S
R	airplane Reynolds number
R_x	Reynolds number on plate, $\frac{Ux}{\nu}$
R_w	Reynolds number of slot, $\frac{Uw}{\nu}$
r	radius of pipe
S	area of surface
T	temperature

U	velocity outside boundary layer
u	velocity inside boundary layer and parallel to surface
$\bar{u}$	average velocity in pipe
v	velocity
v^*	friction velocity, $\sqrt{\frac{\tau}{\rho}}$
w	width of slot or scratch
x	distance along surface from leading edge
y	distance in perpendicular direction from surface
μ	viscosity
ν	kinematic viscosity, $\frac{\mu}{\rho}$
ρ	density
τ	shear stress
γ	ratio of specific heats

Subscripts:

h	evaluated at height of roughness
N	Nikuradse data
0	smooth surface
p	pipe
t	total
w	at wall
δ	at outer edge of boundary layer
CW	Colebrook and White data
wing	wing
s	slot

sc	scratch
wa	wetted area
f	fuselage
t_v	vertical tail
t_h	horizontal tail

PROCEDURE

A detailed investigation has been made of the surface roughness and excrescences present on three service airplanes having accumulated service hours of 213, 214, and 25. These airplanes were selected because they are believed to be representative of usual manufacturing practices for high subsonic and transonic airplanes and because wind-tunnel drag data on these configurations were available. The investigation can be divided into the following steps: (1) the minimum size of roughness which would produce drag at flight Reynolds numbers was determined; (2) a careful comparison was made of the wind-tunnel models and the corresponding airplane to discover the drag-producing roughness items present on the airplane but not simulated on the wind-tunnel models; (3) each of the roughness items present on the airplanes but not simulated on the wind-tunnel models was measured and counted; (4) the drag contribution at flight Reynolds number of each of these roughness items was calculated by using available subsonic data; and (5) the roughness drag was added to the model drag extrapolated to full-scale Reynolds numbers and a comparison made of the total drag thus estimated with the drag measured on the full-scale airplane.

Determination of Minimum Size of Roughness

From a study of subsonic and low supersonic literature (for example, refs. 2 to 10), it was found that, for fully turbulent flow and the range of Mach number possible for these airplanes, the roughness would contribute to the skin-friction drag if the roughness Reynolds number exceeded approximately 100. This roughness Reynolds number is a function of roughness height and free-stream velocity, density, and viscosity. With 100 as the critical roughness Reynolds number and the performance characteristics of these airplanes (Mach number 0.9 to 1.50), it was found that any roughnesses larger than 0.0002 inch to 0.0004 inch present on the airplane would contribute to the airplane drag.

Roughnesses on Airplane Not Simulated on Models

With the minimum size for roughness (0.0002 inch to 0.0004 inch) which will contribute to the turbulent skin-friction drag, a comparison was made of typical scale models (examples of which are shown in fig. 1) with the corresponding airplanes (fig. 2) and it was found that the following roughnesses are not usually simulated on the scale models: rivets, screws and other fasteners, butt and lap joints, hinges of all types, gaps around the high lift or control surfaces, and small projections or indentations such as aerials, steps, handholds, ammunition chutes, and pitot probes. In addition to the more obvious physical differences there are myriads of tiny pits and scratches in the metal surfaces of the airplane which are larger than the specified 0.0002 inch to 0.0004 inch. It may be argued that there are similar pits and scratches on the model surfaces; however, with a critical Reynolds number of 100, a scratch on the model must be on the order of 0.004 inch to 0.008 inch or more to be effective at the model Reynolds number and the finishes of most models are such as to preclude all but a few such scratches. Therefore, when considering whether a roughness item is simulated on the model, one must also consider its Reynolds number as well as its physical presence. For example, if the rivets and butt joints of an airplane were simulated on a 1/20-scale model, the scale Reynolds number of these items might well be less than 100; thus, the surface would be aerodynamically smooth even though the defects are physically simulated on the model.

Measurement and Tabulation of Roughness

After the minimum size of roughness which must be measured and the physical differences between the model and the airplane were determined, it was then necessary to measure and count each of the drag-producing roughness items present on the three airplanes selected for this investigation. For such roughness items as hinges, butt joints, projections, control-surface gaps, holes, and other relatively large surface discontinuities, it was a simple matter to obtain the physical dimensions and total number of each. For the rivets, spot welds, pits, and scratches, expediency required the use of a statistical averaging process to obtain the size and total number of each. (A sufficiently large number of areas were taken so that the addition of other areas did not affect the average per area.) With an average count per unit area and a knowledge of the total wetted area of the airplane, the total for the airplane was then estimated. The accuracy of this procedure was checked by obtaining the total number of rivets on airplane B by this method and by actual count. The totals thus obtained were 47,889 and 49,003, respectively.

Besides the width and length of the small scratches (obtained with a 15-power microscope), it is necessary to know the depth of the scratch in order to calculate its drag contribution. Attempts were made to obtain this measurement by taking casts of the surface and by use of shadowgraphs and, although neither method proved to be entirely satisfactory, they did indicate that, in general, the depth of such small scratches was approximately one-half the width. This value, therefore, was used for subsequent drag calculations.

A listing of the various types of roughnesses measured on the three airplanes is given in table I.

Drag Calculation of Roughness Elements

The drag of the various roughness elements found on the airplanes but not simulated on the models (see table I) was evaluated by the use of low-speed data obtained from reference 10 and are presented in table I. In calculating the drag of the scratches and pits on the metal surfaces of the airplanes, the data presented in reference 10 for slot data were used. These data, however, are for slots whose widths and depths are large in comparison with the boundary-layer thickness and, therefore, the use of these data is questionable when applied to scratches of the type considered herein which are small relative to the boundary-layer thickness. For this reason, the drag of these small scratches was also determined by the method presented in the appendix and the results are presented in table I. The method presented in the appendix is based on the following assumption: For scratches which are small relative to the boundary-layer thickness, the shape of the drag curves as a function of the ratio of boundary-layer thickness to scratch depth is the same as for a sand-type roughness. Admittedly, such an assumption may be in error; however, it was thought that such an analysis would result in more accurate drag values for these small scratches than would be obtained by the use of the data presented in reference 10.

The scratch drags as calculated by use of the appendix are presented in table I and are approximately one-third of those calculated by the data presented in reference 10. The scratch-drag contribution by either method is small, however, and for this reason it is suggested that the more conventional method using data from reference 10 be used until such time as experimental evidence can be obtained to substantiate the assumptions made in the appendix.

It should be pointed out that, at supersonic speeds, the roughness contribution to drag will be at least as large as at subsonic speeds, and in all probability larger, because of the additional wave drag. It was estimated for the present airplanes, however, that the roughness

wave-drag increment is only a small percentage of the total roughness drag as calculated from the low-speed data of reference 10. For full supersonic or hypersonic aircraft, however, roughness-drag data obtained supersonically should be used for a more accurate evaluation. There are, at present, a limited amount of these data available. (See, for example, refs. 6 to 9.) Another point to consider with regard to such calculations for supersonic airplanes is that the roughness items of greatest importance for these airplanes may be different from those considered for the airplanes of the present investigation.

Reduction of Model Data

A careful appraisal of the three airplanes selected for this investigation indicated there would be little or no laminar flow obtained in flight; therefore, only fully developed turbulent flow conditions were considered in this analysis. Because of variations in testing procedures, it is quite possible that some of the models tested did have limited areas of laminar flow. The model data were obtained from references 11 to 16 and other sources of limited availability. Only those data which careful inspection appeared to indicate limited extents of laminar flow were used in the present analysis. With the assumption of fully turbulent flow conditions for these results, the model data were extrapolated to full-scale Reynolds numbers by use of the turbulent skin-friction drag curves presented in reference 3. As in other investigations of a similar nature (for example, ref. 2), it is assumed that only the skin-friction drag coefficient is affected by Reynolds number changes, that is, all other drag components such as wave drag, interference drag, or drag due to lift are assumed to be invariant with Reynolds number. The Reynolds number correction to the skin friction was accomplished by taking representative lengths of the four main components of the airplane (wing, fuselage, horizontal tail, and vertical tail) and calculating a model and full-scale Reynolds number for each of these items. Then for each Reynolds number a corresponding skin-friction drag coefficient $C_{D,f}$ was obtained from reference 3. The difference between $C_{D,f}$ at the model Reynolds number and $C_{D,f}$ at the full-scale Reynolds number was then converted to an incremental drag coefficient based on wing area with the following relation:

$$\left[\left(C_{D,f}\right)_{model} - \left(C_{D,f}\right)_{full\ scale}\right] \frac{S_{wa}}{S_{wing}} = \Delta C_D$$

This conversion is made for each of the components and then the total skin-friction drag decrement is

$$\Delta C_{D,t} = \Delta C_{D,wing} + \Delta C_{D,f} + \Delta C_{D,t_h} + \Delta C_{D,t_v}$$

Inasmuch as it was assumed that all other components of the total drag were unaffected by Reynolds number, $\Delta C_{D,t}$ is the amount by which the model drag will be reduced by this extrapolation or

$$(C_D)_{model} - \Delta C_{D,t} = (C_D)_{model \text{ at full-scale } R}$$

To obtain the predicted airplane drag, the drag contribution of the roughnesses is then added to the extrapolated model drag; thus

$$(C_D)_{model \text{ at full-scale } R} + (C_D)_{roughness} = (C_D)_{airplane \text{ estimated}}$$

This method of obtaining a predicted airplane drag coefficient from a combination of model data and an evaluated drag of roughness elements present on an airplane but not simulated on the model is graphically illustrated in figure 3.

DISCUSSION OF RESULTS

Table I presents in coefficient form the drags as calculated by use of the data of reference 10 for the roughness elements present on the airplane but not simulated on the model. Also shown in table I is the scratch drag as calculated by the method presented in the appendix of this report. From table I it is seen that the drag contribution of each type element is relatively small; however, the total drag of all roughness elements represents an important percentage of the airplane drag. In addition to the roughness elements presented in table I, leakage of air through the airplane surfaces may also be a significant drag item, but the magnitude of this effect could not be estimated from a visual inspection of the airplanes.

Comparisons between the drag coefficients measured on the full-scale airplanes and those estimated from model tests in accordance with the procedure outlined in this report are made in figure 4. The model data were obtained from references 11 to 16 and other sources of limited availability. Full-scale data were obtained from references 17 to 20.

To explain figure 4 more fully, let us consider one of the curves presented in figure 4(a) for $M \leqq 0.8$. By starting with the model drag coefficient at a Reynolds number of 5×10^6, the coefficient is extrapolated by means of the turbulent skin-friction law (ref. 3) to full-scale Reynolds number of 4.2×10^7. (The line joining the model data

point to the extrapolated data point is for guidance only and does not represent the drag coefficients at intermediate values of the Reynolds number.) At the full-scale Reynolds number, the extrapolated drag coefficient is increased by the roughness drag (indicated by the short dashed line at the arrowhead). The predicted airplane drag may then be compared with the full-scale airplane drag as measured in flight (shown by the crosshatched band).

At this time it may be well to discuss the factors which contribute to the scatter of data presented in figures 4(a) and 4(c). A review of the references from which the model data were obtained indicates considerable variations in testing techniques for the various investigations. The more obvious differences were: (1) position of transition, either fixed or natural; (2) methods used to correct for internal flows; (3) corrections for sting interferences; (4) surface finish; and (5) accuracy with which the data were measured and reduced. It is apparent, then, that accurate evaluations of full-scale aircraft drag requires very careful experimentation in the wind tunnel as well as consideration of the full-scale airplane roughness drag. The rather wide band of data measured in flight is normal for flight investigations and is principally due to the difficulty in measuring engine thrust, true airspeed, and angle of attack.

Despite the scatter in available model and flight data, the agreement between the predicted and flight drags shown in figure 4 is sufficiently good to indicate that this method of predicting flight drags from model data is basically correct. Furthermore, the results presented in figure 4(b) show close agreement between predicted drags and the full-scale drags where both the model and airplane tests were conducted in wind tunnels under carefully controlled physical and aerodynamic conditions. It becomes apparent, then, that, if sufficient care is taken in model simulation of the full-scale configuration and in wind-tunnel testing techniques, the accuracy with which full-scale drags may be estimated from model tests is dependent upon the accuracy with which the drag-producing elements present on the airplane but not simulated on the model are evaluated.

CONCLUDING REMARKS

A quantitative evaluation of the surface defects existing on three different operational airplanes indicated an appreciable drag contribution of these defects to the total drag of the airplanes. It was shown that, for airplanes having little laminar flow, a rational approach to the prediction of the full-scale airplane drag consists of extrapolating to full-scale Reynolds numbers according to the turbulent skin-friction

law values of model drag measured with transition fixed near the component leading edges and then adding an estimated drag of those drag-producing elements present on the airplane but not simulated on the model. The accuracy of the final drag prediction is, of course, dependent upon the accuracy of the model drag measurements and the measurement and evaluation of the surface defects on the airplanes. Although the present investigation was made for transonic and high subsonic speed aircraft, the same method should be applicable to supersonic aircraft providing supersonic model and roughness-drag data are used in the evaluation.

Langley Research Center,
National Aeronautics and Space Administration,
Langley Air Force Base, Va., December 18, 1961.

APPENDIX

ANALYSIS OF DRAG DUE TO SURFACE SCRATCHES

The purpose of this analysis is to estimate the difference in drag coefficient between a surface without scratches and a surface with scratches when the scratches have widths ranging from about 0.0003 inch to about 0.005 inch and vary in angle to the airstream from 0° to 90°. The estimate is made from the data for the drag coefficients of single slots of rectangular cross section with widths between 0.3 inch and 2 inches. (See ref. 21.) Part of the data for the slots are given for the complete range of angles between 0° and 90° to the stream but only the data for slots parallel to or perpendicular to the stream are used in the analysis because, in the measurements of the scratches on an airplane, all scratches that were at an angle between 0° and 45° to the airstream were assumed to be parallel to the airstream and all scratches that were at an angle between 45° and 90° to the airstream were assumed to be perpendicular to the airstream.

The present analysis is approximate and is not substantiated by experimental values for the drag of "scratched surfaces"; however, it is believed that this approximation is considerably more accurate than would be the case if the data for the large slots (ref. 10) were used.

ANALYSIS

Incompressible Flow

Because the narrowest slot (ref. 21) is about 60 times as wide as the widest scratch it is necessary to determine the variables on which the drag of a slot or a scratch depends before the drag of a scratch can be calculated from the measured drag of a slot. The problem is how to extrapolate the experimental data for the slots down to the scratches which are very much narrower.

In reference 21 are shown sketches of the flow pattern when rectangular slots are cut into a flat plate. The sketches indicate and the statement is made in the text that the flow pattern is almost independent of the thickness of the boundary layer. In the present analysis the assumption is therefore made that the drag of a slot does not depend on the boundary-layer thickness. For a fixed ratio of slot depth to slot width the drag per unit length of slot is assumed to depend on the velocity near the surface of the plate, on the depth of the slot, and

on the density and viscosity of the fluid. The ratio of the slot length to depth and the angle between the center line of the slot and the airstream are assumed to be parameters.

Near the surface, the velocity is given approximately by $\left(\frac{\partial u}{\partial y}\right)_w y$ or, what is the same thing, by $\frac{\tau_w}{\mu} y$. Therefore, the velocity near the surface is proportional to τ_w. The drag of a slot is thus assumed to depend on τ_w, h, μ, and ρ. The assumption of a relation between D_s, τ_w, h, μ, and ρ; and the use of a dimensional analysis (ref. 22) leads to the result that

$$\frac{D_s}{\mu v^*} = f_r\left(\frac{hv^*}{\nu}\right) \tag{A1}$$

The value of τ_w varies in the neighborhood of a slot or other distortion of the surface. There is thus a question as to where the value of τ_w should be taken. This question can, however, be avoided by noting that the flow over a surface distortion or a pattern of surface distortions is uniquely determined by the distortion or distortions and the distortion free flow. Consequently, the quantities v^*, μ, and ν in equation (A1) can be replaced by the values for the smooth surface. Equation (A1) then becomes

$$\frac{D_s}{\mu_0 v_0^*} = f\left(\frac{hv_0^*}{\nu_0}\right) \tag{A2}$$

The function f in equation (A2) is unknown; if it were known, the drag of any slot of known geometry could be calculated. In the present analysis the function $f(\ )$ is to be found by use of experimental data. To make use of the data of reference 21 which are given in the form of drag coefficients for the slots, the expression (A2) is written in a form that contains the drag coefficient. To do this, a drag coefficient C_D is defined in the same way as in reference 21, namely, as

$$C_D = \frac{D_s}{\frac{\rho}{2} U^2{}_w} \tag{A3}$$

When the definition (eq. (A3)) is combined with equation (A2), the result is

$$C_D = \frac{2}{R_w}\sqrt{\frac{\tau_{w,0}}{\rho U^2}}\, f\left(\frac{hv_0^*}{\nu_0}\right) \tag{A4}$$

where the substitutions $\sqrt{\frac{\tau_{w,0}}{\rho U^2}} = \frac{v_0^*}{U}$ and $R_w = \frac{U_w}{\nu_0}$ are made. By noting that $\frac{hv_0^*}{\nu_0} = \frac{h}{w}\frac{wv_0^*}{\nu_0} = \frac{h}{w} R_w \sqrt{\frac{\tau_{w,0}}{\rho U^2}}$ equation (A4) can be written as

$$C_D = \frac{2}{R_w}\sqrt{\frac{\tau_{w,0}}{\rho U^2}}\, f\left(\frac{h}{w} R_w \sqrt{\frac{\tau_{w,0}}{\rho U^2}}\right) \tag{A5}$$

The numerical value of the function f can then be calculated by

$$f\left(\frac{h}{w} R_w \sqrt{\frac{\tau_{w,0}}{\rho U^2}}\right) = \frac{C_D R_w}{2\sqrt{\frac{\tau_{w,0}}{\rho U^2}}} \tag{A6}$$

The data for slots in references 21 and 23 are used to calculate the value of the function f (the function for slots). The ratio of depth to width h/w is a parameter. The result of these calculations for slots perpendicular to or parallel to the airstream are given in tables II and III.

A calculation of the value of $\frac{hv_0^*}{\nu_0}$ for a typical scratch, namely, one that is 0.003 inch wide and 0.0015 inch deep and is 4 feet from the leading edge of a plate moving at 1,115 feet per second at sea level results in a value of about 30 for $\frac{hv_0^*}{\nu_0}$. Therefore, the values of f for the slots with $\frac{h}{w} = \frac{1}{2}$ must be extrapolated from known values of about 708 (table II) down to values of at least as small as 30. The only known experimental data with values of $\frac{hv_0^*}{\nu_0}$ less than 30 seem to be the data obtained by Nikuradse (ref. 24) and by Colebrook and White (ref. 25) for the friction of sand-covered pipes. The "sand data" are shown in figures 41 and 47 of reference 21 where it is indicated that the drag coefficient for a depression is not very different from the

drag coefficient of a projection of the same shape when the depth of the depression and the height of the projection both approach zero. Because the drag of a depression is almost independent of the boundary-layer thickness, it follows that the drag of a surface projection of very small height is also almost independent of the boundary-layer thickness. This conclusion permits the assumption to be made that for sufficiently small heights of projections the drag of a projection depends only on τ_w, h, μ, and ρ.

Consequently, the drag of a small projection depends on the same variables as the drag of a small depression. The dimensional analysis that leads to equation (A2) is thus applicable to projections as well as to depressions with the result that

$$\left(\frac{D_s}{\mu_0 v_0^*}\right)_p = F\left(\frac{hv_0^*}{\nu_0}\right) \tag{A7}$$

where $F\left(\frac{hv_0^*}{\nu_0}\right)$ seems to become equal to $f\left(\frac{hv_0^*}{\nu_0}\right)$ for $\left(\frac{hv_0^*}{\nu_0}\right)$ approaches 0.

To use the sand data to extrapolate the slot data to the values of $\frac{hv_0^*}{\nu_0}$ that scratches have, the assumption is made that the shape of f for a scratch as a function of $\frac{hv_0^*}{\nu_0}$ is the same shape as the function of F with $\frac{hv_0^*}{\nu_0}$ for sand roughness. To obtain the shape of the curve F against $\frac{hv_0^*}{\nu_0}$, consider a surface of area S on which there are n projections. Then the relation between the average shear stress τ_w of the area S with the projections and the average shear stress of the area S without the projections is

$$\tau_w S = \tau_{w,0} S + D_s L n \tag{A8}$$

where D_s is the drag per unit length of projection perpendicular to the stream. (See fig. 5.) Equation (A8) defines the drag D_s which

depends on the projection particle geometry and spacing. Then

$$\tau_w = \tau_{w,0} + D_s L\left(\frac{n}{S}\right) \tag{A9}$$

Now let $\frac{n}{S} = N$, the number of projections per unit area. Then equation (A9) becomes

$$\tau_w = \tau_{w,0} + D_s LN \tag{A10}$$

or

$$D_s = \frac{\tau_w - \tau_{w,0}}{LN} \tag{A11}$$

From equation (A7) $D_s = \mu_0 v_0^* F\left(\frac{hv_0^*}{\nu_0}\right)$; therefore equation (A11) becomes

$$\mu_0 v_0^* F\left(\frac{hv_0^*}{\nu_0}\right) = \frac{\tau_w - \tau_{w,0}}{LN} = D_s \tag{A12}$$

or

$$F\left(\frac{hv_0^*}{\nu_0}\right) = \frac{hv_0^*}{\nu_0} \frac{1}{LNh}\left[\frac{\rho}{\rho_0}\left(\frac{v^*}{v_0^*}\right)^2 - 1\right]$$

$$F\left(\frac{hv_0^*}{\nu_0}\right) = \frac{hv_0^*}{\nu_0} \frac{w}{h} \frac{1}{LNw}\left[\frac{\rho}{\rho_0}\left(\frac{v^*}{v_0^*}\right)^2 - 1\right] \tag{A13}$$

Now consider the term LNw. The projected area of one distortion, in particular of a grain of sand, is CwL. (See fig. 5.) Then CwLN is the projected area of the distortion per unit area; call this C_1. Thus

$$CLNw = C_1$$

or

$$LNw = \frac{C_1}{C}$$

Equation (A13) then becomes

$$F\left(\frac{hv_0^*}{\nu_0}\right) = \frac{w}{h}\,\frac{C}{C_1}\,\frac{hv_0^*}{\nu_0}\left[\frac{\rho}{\rho_0}\left(\frac{v^*}{v_0^*}\right)^2 - 1\right] \tag{A14}$$

The ratio $\frac{w}{h}$ and the ratio $\frac{C}{C_1}$ are parameters that depend on geometry of the grains of sand and their packing. The ratios $\frac{\rho}{\rho_0}$ and $\frac{v^*}{v_0^*}$ depend only on $\frac{hv_0^*}{\nu_0}$. $\left(\text{For incompressible flow } \frac{\rho}{\rho_0} = 1.\right)$

Because only the shape of the F curve is needed, it is not necessary to know $\frac{w}{h}$ or $\frac{C}{C_1}$. The shape of the curve can be obtained by calculating FC_2, where $C_2 = \frac{h}{w}\,\frac{C_1}{C}$. To calculate the ratio $\frac{v^*}{v_0^*}$, use is made of the information in references 24 and 25, which are for incompressible flows. From equation (A9) of reference 24 with the constant 0.8 replaced by 0.706 (see ref. 25), it follows that,

$$\frac{rv_0^*}{\nu_0} = \frac{\left(\frac{\bar{u}r}{\nu}\right)_0}{2.83\left[0.706 + 2\left(\log_{10}\frac{r}{h} + \log_{10}\frac{hv_0^*}{\nu_0}\right)\right]} \tag{A15}$$

From equation (8) of reference 24 it follows that

$$\frac{rv^*}{\nu} = \frac{\left(\frac{\bar{u}r}{\nu}\right)}{2.83\left[2\log_{10}\frac{r}{h} + f_1\left(\log_{10}\frac{hv^*}{\nu}\right)\right]} \tag{A16}$$

Now let the radius r of the pipe, the kinematic viscosity ν, and the average velocity $\bar{u}$ be unchanged by the addition of roughness; the pressure drop and, consequently, the wall friction is not now the same. Then the ratio $\frac{v^*}{v_0^*}$ is obtained by dividing equation (A16) by equation (A15) with the result

$$\frac{v^*}{v_0^*} = \frac{0.706 + 2 \log_{10} \frac{r}{h} + 2 \log_{10} \frac{hv_0^*}{\nu_0}}{2 \log_{10} \frac{r}{h} + f_1\left(\log_{10} \frac{hv^*}{\nu}\right)} \tag{A17}$$

Equation (A17) can be written in a form that is more convenient for calculating $\frac{v^*}{v_0^*}$, namely as,

$$\frac{v^*}{v_0^*} = \frac{0.706 + 2 \log_{10} \frac{r}{h} + 2 \log_{10} \frac{hv^*}{\nu} + 2 \log_{10} \frac{v_0^*}{v^*}}{2 \log_{10} \frac{r}{h} + f_1\left(\log_{10} \frac{hv^*}{\nu}\right)} \tag{A18}$$

with the assumption $\frac{v}{v_0} = 1$. For a given value of $\frac{r}{h}$, the value of $\frac{v^*}{v_0^*}$ is found by iteration from equation (A18) for each value of $\frac{hv^*}{\nu}$ for which f_1 is given in reference 28.

To find $\frac{hv_0^*}{\nu_0}$ from $\frac{hv^*}{\nu}$ the equation

$$\frac{hv_0^*}{\nu_0} = \left(\frac{hv^*}{\nu}\right)\frac{v_0^*}{v_0} \qquad \left(\frac{\nu_0}{\nu} = 1\right) \tag{A19}$$

is used. By the use of equations (A18), (A19), and (A14) with $\frac{\rho}{\rho_0} = 1$, the function FC_2 is calculated for the data in reference 24. The results are shown in figures 6 and 7.

The values of the ratio $\frac{v^*}{v_0^*}$ for the data for the plates I and V of reference 25 are computed by the use of equation (A18) with the values of f_1 given in reference 25. The values of $\frac{hv_0^*}{\nu_0}$ and FC_2 are then computed by the same method as for the data of reference 24. The results are also shown in figures 6 and 7.

Because the shape of the FC_2-curves (fig. 7) for the different values of r/h do not differ much from one another for the data of reference 28 and because the FC_2-curve for $\frac{r}{h} = 15$ is the only one that extends to sufficiently large values of $\frac{hv_0^*}{\nu_0}$, this curve was chosen to define the shape of the FC_2-curve. The ordinates of the FC_2-curve for $\frac{r}{h} = 15$ were then multiplied by a constant, called B, which depended on h/w and which was determined by the condition that the curve obtained by multiplying the ordinates of the FC_2-curve by B be a "least-squares error" curve for the slot data for a particular value of h/w. The derivation of the formula for calculating the value of the B is as follows. The sum of the squares of the difference between the values of f_s for the slots and the values of BFC_2 for a fixed value of h/w is

$$E = \sum_{m=0}^{M} \left(f_s - BFC_2\right)_m^2$$

where m denotes the mth difference and M represents the maximum number of differences considered. When B has the value to make E a minimum,

$$\frac{\partial E}{\partial B} = \sum_{m=0}^{M} 2\left(f_s - BFC_2\right)_m \left(-FC_2\right)_m = 0$$

or

$$\sum_{m=0}^{M} \left[f_s\left(FC_2\right)\right]_m - B \sum_{m=0}^{M} \left(FC_2\right)_m^2 = 0$$

or

$$B = \frac{\sum_{m=0}^{M} \left[f_s\left(FC_2\right)\right]_m}{\sum_{m=0}^{M} \left(FC_2\right)_m^2} \tag{A20}$$

The final curve of f against $\frac{hv_0^*}{\nu_0}$ is then obtained by multiplying the FC_2-curve by B. A sample calculation for $\frac{h}{w} = 1$ slots perpendicular to the flow is shown in table IV.

For values of $\frac{hv_0^*}{\nu_0} < 4$ a least-squares error straight line was placed through the origin and the values of FC_2 were calculated from reference 24. The equation of the line was obtained by noting that the equation of every line through the origin is

$$FC_2 = a \frac{hv_0^*}{\nu_0}$$

The sum of the squares of the differences between this line and the data points for $\frac{hv_0^*}{\nu_0} < 4$ is

$$E = \sum_{m=0}^{M} \left(FC_2 - a \frac{hv_0^*}{\nu_0}\right)_m^2$$

For E to be a minimum

$$\frac{\partial E}{\partial a} = \sum_{m=0}^{M} 2\left(FC_2 - a\,\frac{hv_0^*}{\nu_0}\right)_m \left(-\,\frac{hv_0^*}{\nu_0}\right)_m = 0$$

or

$$a = \frac{\sum_{m=0}^{M} \left(FC_2\,\frac{hv_0^*}{\nu_0}\right)_m}{\sum_{m=0}^{M} \left(\frac{hv_0^*}{\nu_0}\right)_m} \tag{A21}$$

The value of a was found to be 0.02269. The least-squares straight line is shown in figure 6. It is remarked that the relation $FC_2 = a\,\frac{hv_0^*}{\nu_0}$ for $\frac{hv_0^*}{\nu_0} < 4$ is the result of choosing a straight line through $FC_2 = 0$, $\frac{hv_0^*}{\nu_0} = 0$ as a fairing for the data for $\frac{hv_0^*}{\nu_0} < 4$; these data have a large amount of scatter. One consequence of a straight-line fairing is that the drag of a sand grain approaches zero linearly with h as h approaches 0. Thus, from

$$D_s = \mu_0 v_0^*\, F\left(\frac{hv_0^*}{\nu_0}\right)$$

and

$$FC_2 = a\,\frac{hv_0^*}{\nu_0}$$

it follows that

$$D_s = \mu_0 v_0^* \frac{a}{C_2}\left(\frac{hv_0^*}{\nu_0}\right) = \frac{ah}{C_2}\tau_{w,0}$$

with C_2 constant. This expression for D_s can also be written as

$$D_s = \frac{a}{C_2} h\mu_0\left(\frac{\partial u}{\partial y}\right)_{w_0}$$

or with the approximation that $u_h = h\left(\frac{\partial u}{\partial y}\right)_{w_0}$

$$D_s = \frac{a}{C_2}\mu_0 u_h$$

This form for D_s is the same as that for the drag of a cylinder, sphere, or elliptic cylinder when the Reynolds number is small. (See ref. 26.) According to reference 3, this form is accurate for a sphere or cylinder when the Reynolds number based on the diameter and on the velocity at infinity is less than unity. Although the velocity in the expression for D_s is that at the top of the projection instead of at infinity, reference 27 suggests that, when the roughness density is small, the drag of a surface projection can sometimes be calculated by using the drag coefficient for the surface projection in free flow and a velocity equal to the velocity at the top of the projection. The form of the expression for D_s thus seems to be reasonable.

Although the drag of a sand grain approaches zero as $\frac{hv_0^*}{\nu_0}$ approaches zero, the present results indicate that the shear stress of a rough pipe remains slightly greater than that of a smooth pipe. Thus, from

$$FC_2 = \frac{hv_0^*}{\nu_0}\left[\frac{\rho}{\rho_0}\left(\frac{v^*}{v_0^*}\right)^2 - 1\right]$$

and

$$FC_2 = a\frac{hv_0^*}{\nu_0} \qquad \left(\frac{hv_0^*}{\nu_0} < 4\right)$$

it follows that

$$a = \frac{\rho}{\rho_0}\left(\frac{v^*}{v_0^*}\right)^2 - 1$$

or

$$a = \frac{\tau_w}{\tau_{w,0}} - 1$$

or

$$\frac{\tau_w}{\tau_{w,0}} = 1 + a \qquad \left(\frac{hv_0^*}{\nu_0} < 4\right)$$

The reason for this result is that, by taking C_2 to be constant ($C_2 = hLN$), the result of letting h approach 0 is that LN approaches ∞. That is, if the grain size were to approach zero, the total length of the grains normal to the stream would approach infinity. If $\frac{hv_0^*}{\nu_0}$ approaches 0 by letting the velocity through the pipe approach zero, the result seems more plausible; this is the way the experiments were conducted.

In any case, the result that the shear stress of the rough pipe is always slightly greater than that of the smooth pipe does not agree with the conclusion of reference 24 that for values of $\frac{hv^*}{\nu}$ less than 3.5 the shear stress is the same as the shear stress for the smooth pipe. (See eq. 21(a), ref. 24.) The difference, however, is only about 2 percent. It is not clear whether this slight difference is caused by the use of the straight-line fairing down to $\frac{hv_0^*}{\nu_0} = 0$, by a slight inaccuracy in the friction formula for the smooth pipe, by a slight inaccuracy in the measurements for the rough pipe, or whether the friction of the rough pipe is always greater than that of the smooth pipe ($\bar{u}$ approaching 0, h not approaching 0). The slight difference in friction between the smooth and rough pipe for small $\frac{hv^*}{\nu}$ can be noticed in figure 11 of reference 24.

The method of obtaining the f-curves for the slots or scratches will now be discussed. For each value of h/w, f for $\frac{hv_0^*}{\nu_0} < 4$ is represented by a different straight line. The line for a particular value of h/w is obtained by multiplying the slope of the line shown in figure 6 by the value of B for the value of h/w. The final curves of f against $\frac{hv_0^*}{\nu_0}$ for the slots perpendicular to the stream are shown in figure 8.

To obtain some estimate of the change in the calculated drag of slots that would result if an FC_2-curve other than that for $\frac{r}{h} = 15$ (data from ref. 24) were used, the final f-curves for the different values of h/w were recalculated by making use of the FC_2-curve for $\frac{r}{h} = 7.6$ (data from ref. 25). This FC_2-curve differs more from the FC_2-curve for $\frac{r}{h} = 15$ than any of the other curves. (See fig. 8.) The final f-curves based on the $\frac{r}{h} = 7.6$ curve (data from ref. 24) are also shown in figure 8. The difference between the two sets of curves seems to be appreciable for certain ranges of $\frac{hv_0^*}{\nu_0}$.

The same procedure was followed to obtain the final f-curves for the the slots parallel to the flow. These curves are shown in figure 9 both for the $\frac{r}{h} = 15$ (ref. 24) reference curve and for the $\frac{r}{h} = 7.6$ (ref. 25) reference curve.

The object of the analysis, namely, a method for extrapolating the values of f calculated from the measurements on slots for large values of $\frac{hv_0^*}{\nu_0}$ to the much smaller values of $\frac{hv_0^*}{\nu_0}$ associated with scratches, has thus been attained.

Compressible Flow

Although the preceding analysis has been made for incompressible flow, equation (A2) can be extended to compressible flow. If the fluid

properties are variable, then ρ and μ are the fluid properties at the surface. For slots this is clear from the derivation of equation (A2); for projections the values of ρ and μ are somewhere between the surface and $y = h$. For simplicity ρ and μ may also be taken at the surface for projections. The expression (A2) then is

$$\frac{D_s}{\mu_{w,0} v_0^*} = f\left(\frac{h v_0^*}{\nu_{w,0}}\right)$$

where

$$v_0^* = \sqrt{\frac{\tau_{w,0}}{\rho_{w,0}}}$$

Then if

$$C_{D,s} = \frac{D_s}{\frac{\rho_\delta}{2} U^2{}_w}$$

it follows that

$$C_{D,s} = \frac{2\mu_w v_0^*}{\rho_\delta U^2{}_w} f\left(\frac{h v_0^*}{\nu_{w,0}}\right)$$

or

$$C_{D,s} = 2 \frac{\mu_w}{\mu_\delta} \frac{\mu_\delta}{\rho_\delta U_w} \frac{v_0^*}{U} f\left(\frac{h}{w} \frac{wU}{\nu_{\delta,0}} \frac{\nu_{\delta,0}}{\nu_{w,0}} \frac{v_0^*}{U}\right)$$

or

$$C_{D,s} = 2\left(\frac{\mu_w}{\mu_\delta}\right)_0 \frac{1}{R_w}\left(\sqrt{\frac{\rho_\delta}{\rho_w}}\right)_0 \sqrt{\frac{\tau_{w,0}}{\rho_\delta U^2}} f\left[\frac{h}{w} R_w \left(\frac{\rho_w}{\mu_w}\right)_0 \left(\frac{\mu_\delta}{\rho_\delta}\right)_0 \sqrt{\frac{\tau_{w,0}}{\rho_\delta U^2}} \left(\sqrt{\frac{\rho_\delta}{\rho_w}}\right)_0\right]$$

or

$$C_{D,s} = \frac{2}{R_w} \sqrt{\frac{\tau_{w,0}}{\rho_\delta U^2}} \left(\frac{\mu_w}{\mu_\delta}\right)_0 \left(\sqrt{\frac{\rho_\delta}{\rho_w}}\right)_0 f\left[\frac{h}{w} R_w \sqrt{\frac{\tau_{w,0}}{\rho_\delta U^2}} \left(\frac{\mu_\delta}{\mu_w}\right)_0 \left(\sqrt{\frac{\rho_w}{\rho_\delta}}\right)_0\right]$$

but $\frac{\rho_\delta}{\rho_w} = \frac{T_w}{T_\delta}$, then

$$C_{D,s} = \frac{2}{R_w}\sqrt{\frac{\tau_{w,0}}{\rho_\delta U^2}}\left(\frac{\mu_w}{\mu_\delta}\right)_0\left(\sqrt{\frac{T_w}{T_s}}\right)_0 f\left[\frac{h}{w} R_w \sqrt{\frac{\tau_{w,0}}{\rho_\delta U^2}}\left(\frac{\mu_\delta}{\mu_w}\right)_0\left(\sqrt{\frac{T_\delta}{T_w}}\right)_0\right] \tag{A22}$$

If the Sutherland formula (ref. 28) is used to calculate the ratio $\frac{\mu_w}{\mu_\delta}$, the result is

$$\frac{\mu_w}{\mu_\delta} = \frac{1 + \frac{K}{T_\delta}}{1 + \frac{K}{T_\delta}\left(\frac{T_\delta}{T_w}\right)}\sqrt{\frac{T_w}{T_\delta}}$$

Then

$$C_{D,s} = \frac{2}{R_w}\sqrt{\frac{\tau_{w,0}}{\rho_\delta U^2}}\left(\frac{T_w}{T_\delta}\right)_0\left(\frac{1 + \frac{K}{T_\delta}}{1 + \frac{K}{T_\delta}\left(\frac{T_\delta}{T_w}\right)_0}\right) f\left[\frac{h}{w} R_w \sqrt{\frac{\tau_{w,0}}{\rho_\delta U^2}}\left(\frac{T_\delta}{T_w}\right)_0\left(\frac{1 + \frac{K}{T_\delta}\left(\frac{T_\delta}{T_w}\right)}{1 + \frac{K}{T_\delta}}\right)\right] \tag{A23}$$

where K can be taken as 205.2° (ref. 27). The variability of the fluid properties appears mainly as the ratio of the temperature at the surface to the temperature at the outer edge of the boundary layer; the Mach number appears in the dependence of $\frac{\tau_{w,0}}{\rho_\delta U^2}$ on the Mach number.

Because the function f depends only on $\frac{hv_0^*}{\nu_0}$, the slot data obtained for constant property flow can also be used when the fluid properties are variable; that is, figures 8 and 9 are also applicable to variable fluid property flows. For variable fluid property flow

$$\frac{hv_0^*}{\nu_{w,0}} = \frac{h}{w} R_w \sqrt{\frac{\tau_{w,0}}{\rho_\delta U^2}}\left(\frac{T_\delta}{T_w}\right)_0\left(\frac{1 + \frac{K}{T_\delta}\left(\frac{T_\delta}{T_w}\right)}{1 + \frac{K}{T_\delta}}\right)_0 \tag{A24}$$

Scratch Drag Calculations

The f-curves of figures 8 and 9 will now be used to calculate the drag of scratches on airplane B. The sample calculation is for a Mach number of 0.9 at 35,000 feet. The Reynolds number based on a mean aerodynamic chord of 8.09 feet is 17.66×10^6.

The values of h/w for all the scratches is assumed to be 1/2. The scratch sizes and their areas as measured are as follows:

Scratch width, in.	Area of scratches between 0° and 45° to flow, sq ft	Area of scratches between 45° and 90° to flow, sq ft
0.0003	12.39	12.39
.001	9.54	9.54
.002	6.36	6.36
.003	12.71	12.71
.005	5.30	5.30

The drag coefficient of a scratch is calculated from equation (A5), namely,

$$C_{D,s} = \frac{2}{R_w}\sqrt{\frac{\tau_{w,0}}{\rho U^2}}\, f\left(\frac{h}{w} R_w \sqrt{\frac{\tau_{w,0}}{\rho U^2}}\right)$$

The assumption is made that it is sufficiently accurate to take the value of $\frac{\tau_{w,0}}{\rho U^2}$ as that at the center of the mean aerodynamic chord. The value of $\frac{\tau_{w,0}}{\rho U^2}$ is then calculated by Falkner's formula (ref. 3). (All compressibility effects are neglected.) The formula is

$$\frac{\tau_{w,0}}{\rho U^2} = \frac{0.0131}{(R_x)^{1/7}}$$

or with

$$R_x = \frac{17.66}{2} = 8.83$$

$$\frac{\tau_{w,0}}{\rho U^2} = 0.001333$$

The f-curves have been computed by defining the width w as the smallest dimension in the planview. The width w is thus the same whether the slot is parallel or perpendicular to the flow. The calculation is summarized in the following tables. The subscript N means "based on the f-curves derived from Nikuradse data"; the subscript CW means "based on the f-curves derived from Colebrook and White's data."

Values for scratches between 0° and 45° to flow (assumed to be parallel to flow) are as follows:

Scratch width, in.	Scratch area, A_{sc}, sq ft	R_w	$\frac{h}{w} R_w$	f_N	f_{CW}	$\frac{2}{R_w}$	C_{D_N}	$C_{D_{CW}}$	$C_{D_N}A_{sc}$	$C_{D_{CW}}A_{sc}$
0.0003	12.39	54.6	0.997	0.0781	0.2865	0.001338	0.0001045	0.000383	0.001295	0.004745
.001	9.54	182	3.32	.2601	.955	.0004012	.0001045	.000383	.000994	.00365
.002	6.36	364	6.64	1.9	6.1	.0002005	.000381	.001224	.00242	.00778
.003	12.71	546	9.97	10.0	15.3	.0001338	.001335	.002043	.01694	.02598
.005	5.30	910	16.61	31.2	38.6	.0000802	.002502	.003095	.01326	.01640

Then the drag coefficient of scratches between 0° and 45° to the flow is

$$\left(C_{D_w}\right)_N = \frac{C_{D,N}A_{sc}}{A_{wing}} = \frac{0.03491}{287.9} = 0.0001213$$

$$\left(C_{D_w}\right)_{CW} = \frac{C_{D,CW}A_{sc}}{A_{wing}} = \frac{0.05856}{287.9} = 0.0002032$$

Values for scratches between 45° and 90° to flow (assumed to be perpendicular to flow) are as follows:

Scratch width, in.	Scratch area, A_{sc}, sq ft	R_w	$\frac{h}{w} R_w$	f_N	f_{CW}	$\frac{2}{R_w}$	C_{D_N}	$C_{D_{CW}}$	$C_{D_N}A_{sc}$	$C_{D_{CW}}A_{sc}$
0.0003	12.39	54.6	0.997	0.0368	0.134	0.001338	0.0000492	0.0001792	0.00061	0.00222
.001	9.54	182	3.32	.1226	.4465	.0004012	.0000492	.0001792	.000469	.00171
.002	6.36	364	6.64	.870	2.80	.0002005	.0001745	.000561	.00111	.003568
.003	12.71	546	9.97	4.00	7.45	.0001338	.000534	.000996	.00678	.01266
.005	5.30	910	16.61	14.9	18.4	.0000802	.001196	.001476	.00634	.00782

The drag coefficient of scratches between 45° and 90° to the flow is

$$\left(C_{D_w}\right)_N = \frac{\sum C_{D,N}A_{sc}}{A_{wing}} = \frac{0.01531}{287.9} = 0.0000532$$

$$\left(C_{D_w}\right)_{CW} = \frac{\sum C_{D,CW}A_{sc}}{A_{wing}} = \frac{0.02798}{287.9} = 0.0000972$$

Then the total drag coefficient is

$$\left(C_{D_w}\right)_N = 0.0001213 + 0.0000532 = 0.0002$$

$$\left(C_{D_w}\right)_{CW} = 0.0002032 + 0.0000972 = 0.0003$$

Note that, although the f_N and f_{CW} values are very different, the final estimate of the scratch drag coefficient is almost the same whether an f-curve based on the Nikuradse data or an f-curve based on the Colebrook and White data is used.

Because of the approximate nature of the analysis the opinion was held that a sufficiently accurate estimate of the magnitude of the scratch drag could be obtained by neglecting compressibility. In order, however, to show the method of calculation when compressibility is considered, the following example is presented:

Slot perpendicular to stream: $w = 0.003$ inch; $\frac{U}{\nu} = 7.11 \times 10^6$; $M_\delta = 1.1$; $\frac{h}{w} = \frac{1}{2}$; and $T_\delta = 520^\circ$ R

$$R_w = \frac{0.003}{12}\left(7.11 \times 10^6\right) = 1{,}777$$

$$\frac{T_w}{T_\delta} = 1 + \frac{\gamma - 1}{2} M_\delta{}^2 = 1.242$$

$$\sqrt{\frac{\tau_{w,0}}{\rho_\delta U^2}} = 0.03358\left(\frac{C_{f_i}}{C_f}\right) = 0.03358(0.9) = 0.0302$$

$\left(\frac{C_{f_i}}{C_f}\right)$ values being obtained from reference 29

$$\frac{hv_0^*}{\nu_{w,0}} = \frac{1}{2}(1{,}777)(0.0302)\frac{1}{1.242}\,\frac{1 + \frac{205.2}{520}\,\frac{1}{1.242}}{1 + \frac{205.2}{520}} = 20.43$$

and

$$f_{N \text{ or } CW} = 25.5$$

Therefore,

$$C_{D,s} = \frac{2}{1,777}(0.0302)(1.242)\frac{1 + \frac{205.2}{520}}{1 + \frac{205.2}{520}\frac{1}{1.242}}(25.5) = 0.00114$$

For the same Mach number and scratch width but neglecting compressibility, the $C_{D,s}$ is about 0.0018 or about 50 percent larger than when compressibility is considered.

Consequently, an increase in the ratio $\frac{T_w}{T_\delta}$ decreases the drag of this slot by an important amount. The amount of the decrease depends on the value of $\frac{hv_0^*}{\nu_{w,0}}$; for example, if $\frac{hv_0^*}{\nu_{w,0}}$ is so small that $f = b\,\frac{hv_0^*}{\nu_{w,0}}$ where $\frac{hv_0^*}{\nu_{w,0}}$ is given in equation (A24), then

$$C_{D,s} = \frac{2}{R_w}\sqrt{\frac{\tau_{w,0}}{\rho_\delta U^2}\left(\frac{T_w}{T_\delta}\right)_0}\;\frac{1 + \frac{K}{T_\delta}}{1 + \frac{K}{T_\delta}\left(\frac{T_\delta}{T_w}\right)_0}\,b\,\frac{h}{w}\,R_w\sqrt{\frac{\tau_{w,0}}{\rho_\delta U^2}\left(\frac{T_\delta}{T_w}\right)_0}\;\frac{1 + \frac{K}{T_\delta}\left(\frac{T_\delta}{T_w}\right)}{1 + \frac{K}{T_\delta}}$$

or

$$C_{D,s} = 2b\,\frac{h}{w}\,\frac{\tau_{w,0}}{\rho_\delta U^2}$$

The only effect of compressibility on very small scratches is thus through the effect on $\frac{\tau_{w,0}}{\rho_\delta U^2}$ alone. For the present example, the effect would consequently decrease from about 40 percent for a wide scratch to about 10 percent for a very narrow scratch.

LIMITATIONS OF METHOD

The method derived here for extrapolating the measured drag of slots to the much smaller slots that are called scratches is approximate and without tests of plates that are duplicates of airplane surfaces that have accumulated scratches no estimate of the exactness of the extrapolation method can be made.

It is well to note, however, that, although the method presented here for calculating the drag of small scratches is approximate, it is believed to be more accurate than using slot data directly. However, the drag of the scratches are sufficiently small that large errors in evaluating the scratch drag would not appreciably affect the total drag estimate. For this reason, it is suggested that until such time as the assumptions used in this analysis can be verified experimentally, the scratch-drag evaluations be made by use of the more conventional data presented in reference 10.

REFERENCES

1. Howell, Robert R., and Braslow, Albert L.: Experimental Study of the Effects of Scale on the Absolute Values of Zero-Lift Drag of Aircraft Configurations at Transonic Speeds. NACA RM L56J29, 1957.

2. Gieseman, Earl Ralph, Jr.: Drag Correlation of Wind-Tunnel and Flight-Test Data in the Transonic Range. Graduate Thesis (1-GAE-55), U.S. Air Force Inst. Tech., Aug. 30, 1955. (Available from ASTIA as AD 81421.)

3. Schlichting, Herman (J. Kestin, trans.): Boundary Layer Theory. McGraw-Hill Book Co., Inc., 1955.

4. Von Doenhoff, Albert E., and Horton, Elmer A.: A Low-Speed Experimental Investigation of the Effect of a Sandpaper Type of Roughness on Boundary-Layer Transition. NACA Rep. 1349, 1958. (Supersedes NACA TN 3858.)

5. Braslow, Albert L., and Knox, Eugene C.: Simplified Method for Determination of Critical Height of Distributed Roughness Particles for Boundary-Layer Transition at Mach Numbers From 0 to 5. NACA TN 4363, 1958.

6. Czarnecki, K. R., Sevier, John R., Jr., and Carmel, Melvin M.: Effects of Fabrication-Type Roughness on Turbulent Skin Friction at Supersonic Speeds. NACA TN 4299, 1958.

7. Czarnecki, K. R., Robinson, Ross B., and Hilton, John H., Jr.: Investigation of Distributed Surface Roughness on a Body of Revolution at a Mach Number of 1.61. NACA TN 3230, 1954.

8. Sevier, John R., Jr., and Czarnecki, K. R.: Investigation of Effects of Distributed Surface Roughness on a Turbulent Boundary Layer Over a Body of Revolution at a Mach Number of 2.01. NACA TN 4183, 1958.

9. Czarnecki, K. R., and Monta, William J.: Pressure Distributions and Wave Drag Due to Two-Dimensional Fabrication-Type Surface Roughness on an Ogive Cylinder at Mach Numbers of 1.61 and 2.01. NASA TN D-835, 1961.

10. Hoerner, Sighard F.: Aerodynamic Drag. Publ. by the author (148 Busteed, Midland Park, N.J.), 1951.

11. Hastings, Earl C., Jr.: Minimum Drag of Four Versions of a Swept-Wing Fighter Airplane Obtained From Flight Tests of Rocket-Boosted Models at Mach Numbers From 0.81 to 1.71. NACA RM L56E25a, 1956.

12. Wainwright, John B., and Rubenstein, Marvin: Report on the Aerodynamic Effects of External Stores on a Wind Tunnel Model XF8U-1 Airplane in the Mach Number Range 0.8 to 1.4. USCEC Rep. 32-1-5, Aerod. Test Lab., NAMTC, Univ. of Southern California, Apr. 28, 1955.

13. Daniels, W., Jr.: Low Speed Wind Tunnel Tests of a 0.20-Scale Simulated Model of the FJ-3 Airplane To Determine the General Stability and Control Characteristics With an Aileron Spoiler Slot Deflector and With Under-Wing Fuel Tanks, Rocket Packages, and Pylons. Rep. No. NA-55-1235, NAAL-313, North American Aviation, Inc., Nov. 16, 1955.

14. Melkus, H. A.: A Series of Wind Tunnel Tests on a 1.8 Percent Scale Model of the McDonnell F-101A in the Wright Air Development Center 10-Foot Wind Tunnel. WADC Tech. Note WCLS 54-24, ASTIA Doc. No. AD 97303, U.S. Air Force, Dec. 1955.

15. Carmel, Melvin M., and Turner, Kenneth L.: Investigation of Drag and Static Longitudinal and Lateral Stability Characteristics of a Model of a 40.4° Swept-Wing Airplane at Mach Numbers of 1.56 and 2.06. NACA RM L56I17a, 1957.

16. Goodson, Kenneth W.: Wind-Tunnel Investigation at High Subsonic Speeds of the Effects on Static Stability Characteristics of Various Modifications to a Swept-Wing Fighter-Type Airplane Model. NACA RM L57A31, 1957.

17. McFadden, Norman M., Rathert, George A., Jr., and Bray, Richard S.: The Effectiveness of Wing Vortex Generators in Improving the Maneuvering Characteristics of a Swept-Wing Airplane at Transonic Speeds. NACA TN 3523, 1955.

18. Anon.: Flight Test Data Results of the F8U-1 Airplane. Rep. No. 10514, Chance Vought Aircraft, Inc., 1956.

19. Messal, T. O.: Model F-101A Airplane. Status of Flight Test Results. Rep. No. 4073 (Contract No. AF 33(600)-26859), McDonnell Aircraft Corp., Apr. 15, 1955.

20. Madden, J. T., Shields, M. E., and Upton, G. T.: Aerodynamic Design Studies on the F8U-1 Airplane. Rep. No. 11134, Chance Vought Aircraft, Inc., Aug. 5, 1957.

21. Wieghardt, K.: Increase of the Turbulent Frictional Resistance Caused by Surface Irregularities. VG 129, British M.A.P. Völkenrode, June 15, 1946.

22. Langhaar, H. L.: Dimensional Analysis and Theory of Models. John Wiley & Sons, Inc., 1951.

23. Tillmann, W.: Additional Measurements of the Drag of Surface Irregularities in Turbulent Boundary Layers. NACA TM 1299, 1951.

24. Nikuradse, J.: Laws of Flow in Rough Pipes. NACA TM 1292, 1950.

25. Colebrook, C. F., and White, C. M.: Experiments With Fluid Friction in Roughened Pipes. Proc. Roy. Soc. (London), ser. A, vol. 161, Aug. 1937, pp. 367-381.

26. Lamb, Horace: Hydrodynamics. Sixth ed., Dover Publications, 1945.

27. Schlichting, H.: Experimental Investigation of the Problem of Surface Roughness. NACA TM 823, 1937.

28. Fluid Motion Panel of the Aeronautical Research Committee and Others: Modern Developments in Fluid Dynamics. Vols. I and II, S. Goldstein, ed., The Claredon Press (Oxford), 1938.

29. Chapman, Dean R., and Kester, Robert H.: Turbulent Boundary-Layer and Skin-Friction Measurements in Axial Flow Along Cylinders at Mach Numbers Between 0.5 and 3.6. NACA TN 3097, 1954.

TABLE I.- SUMMARY OF SURFACE-DEFECT DRAG CONTRIBUTIONS

Roughness due to -	ΔC_D for -		
	Airplane A	Airplane B	Airplane C
Scratches {from reference 10	--------	0.001030	0.000366
Scratches {from appendix A	--------	.000303	.000145
Butt joints	0.000343	.000492	.000366
Gouges	--------	.000002	.000021
Cover plates	--------	.000195	--------
Rivets	.000185	.000168	.000251
Screws	.000005		.000062
Projections	.000231	.000154	.000107
Holes	.000016	.000013	.000405
Slots	--------	.000002	--------
Leading-edge wing gaps	.002010	.000978	--------
Control-surface gaps		.000270	.000486
Hinges	.000030	--------	.000036
Total obtained by using scratch drag from reference 10	0.002820	0.003304	0.002100
Total obtained by using scratch drag from appendix A	.002820	.002577	.001879

TABLE II.- SLOTS PERPENDICULAR TO FLOW (SEE FIG. 11)

$\frac{h}{w} = \frac{3}{2}$		$\frac{h}{w} = 1$		$\frac{h}{w} = \frac{1}{2}$		$\frac{h}{w} = \frac{1}{4}$		$\frac{h}{w} = \frac{1}{8}$	
$\frac{hv_0^*}{\nu_0}$	f_s	$\frac{hv_0^*}{\nu_0}$	f_s	$\frac{hv_0^*}{\nu_0}$	f_s	$\frac{hv_0^*}{\nu_0}$	f_s	$\frac{hv_0^*}{\nu_0}$	f_s
2,415	7,431	2,113	4,305	1,059	6,095	490	8,380	264	8,340
2,125	5,155	1,961	4,490	988	5,735	490	8,940	245	7,610
		1,961	4,600	982	6,615	403	6,240	245	7,470
		1,961	4,515	981	6,710	354	4,930	245	7,510
		1,960	4,480	981	6,380			202	6,675
		1,960	4,822	806	5,405			177	4,575
		1,611	5,300	708	4,410				
		1,417	3,962						
		1,057	1,614						
		980.5	2,412						
		980	2,254						

TABLE III.- SLOTS PARALLEL TO FLOW (SEE FIG. 12)

$\frac{h}{w} = \frac{3}{2}$		$\frac{h}{w} = 1$		$\frac{h}{w} = \frac{1}{2}$		$\frac{h}{w} = \frac{1}{4}$		$\frac{h}{w} = \frac{1}{8}$	
$\frac{hv_0^*}{\nu_0}$	f_s	$\frac{hv_0^*}{\nu_0}$	f_s	$\frac{hv_0^*}{\nu_0}$	f_s	$\frac{hv_0^*}{\nu_0}$	f_s	$\frac{hv_0^*}{\nu_0}$	f_s
2,940	12,130	2,113	16,150	988	13,110	490	5,030	245	2,853
2,415	7,010	1,961	24,780	982	13,310	490	4,575	245	2,958
2,125	8,502	1,961	24,960	981	13,320	403	3,012	202	1,144
		1,960	24,980	806	10,050	354	2,220	177	944
		1,960	24,900	708	9,630				
		1,611	12,300						
		1,417	12,050						
		1,057	4,745						
		980	6,140						
		980	6,282						

TABLE IV.- SAMPLE CALCULATIONS FOR SLOTS PERPENDICULAR TO FLOW; $\frac{h}{w} = 1$ (REFS. 21, 23)

[Nikuradse sand data for $\frac{r}{b} = 15$ (ref. 24)]

$\frac{hv_0^*}{\nu_0}$ (table II)	f_s (table II)	FC_2 (fig. 10)	$f_s(FC_2)$	$(FC_2)^2$
2,113	4,305	9,720	$4,184 \times 10^4$	$9,448 \times 10^4$
1,961	4,490	8,900	3,996	7,921
1,961	4,600	8,900	4,094	7,921
1,961	4,515	8,900	4,018	7,921
1,960	4,480	8,900	3,987	7,921
1,960	4,822	8,900	4,292	7,921
1,611	5,300	7,000	3,710	4,900
1,417	3,962	6,020	2,385	3,624
1,057	1,614	4,250	686	1,806
980.5	2,412	3,840	926	1,475
980	2,254	3,820	861	1,459
			$33,139 \times 10^4$	$62,317 \times 10^4$

$$B = \frac{\sum_{m=0}^{M} \left[f_s(FC_2)\right]_m}{\sum_{m=0}^{M} (FC_2)_m^2} = 0.5318$$

TABLE IV.- SAMPLE CALCULATIONS FOR SLOTS PERPENDICULAR TO FLOW; $\frac{h}{w} = 1$ (REFS. 21, 23) - Concluded

$\frac{hv_0^*}{\nu_0}$	FC_2	$B(FC_2)$
5	0.166	0.088
6	.353	.188
8	1.23	.654
10	2.45	1.303
15	7.10	3.776
20	14.0	7.445
30	32.0	17.02
50	73.5	39.09
100	200	106.4
200	500	265.9
300	850	452.0
400	1,230	654.1
600	2,090	1,111
800	2,980	1,585
1,000	3,950	2,101
1,200	4,930	2,622
1,400	5,950	3,164
1,600	6,980	3,712
1,800	8,000	4,254
2,000	9,100	4,839
2,200	10,200	5,324

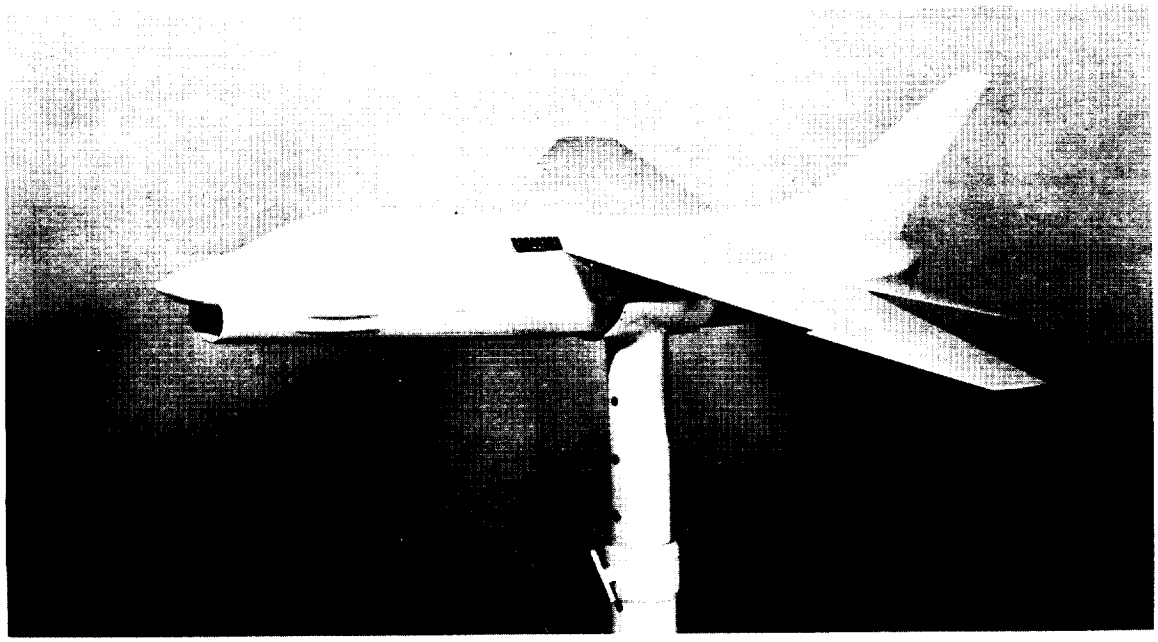

(a) Airplane A. L-82838

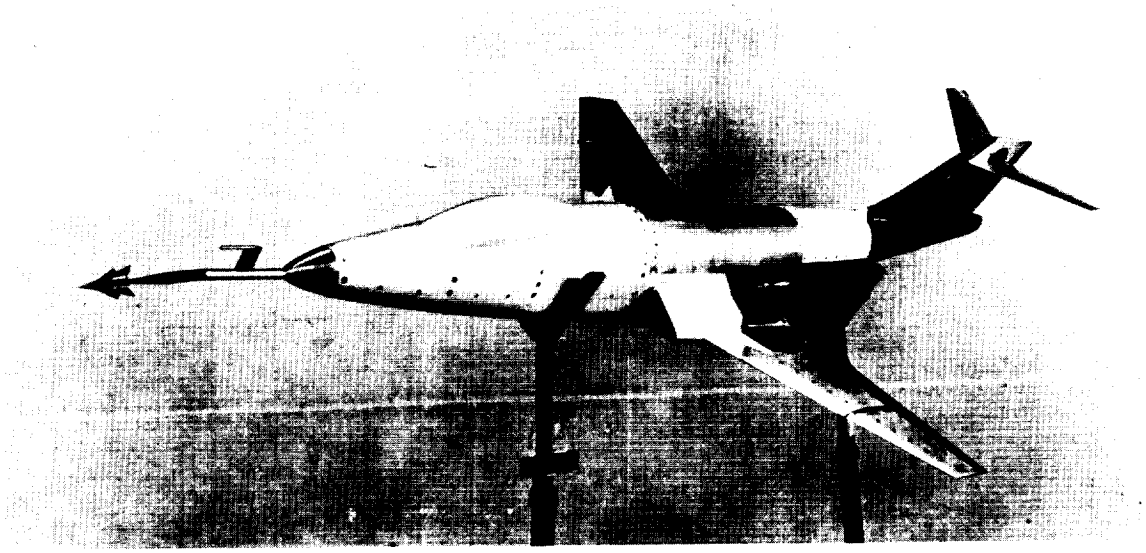

(b) Airplane C. L-86586.1

Figure 1.- Photographs of typical models of airplanes A and C.

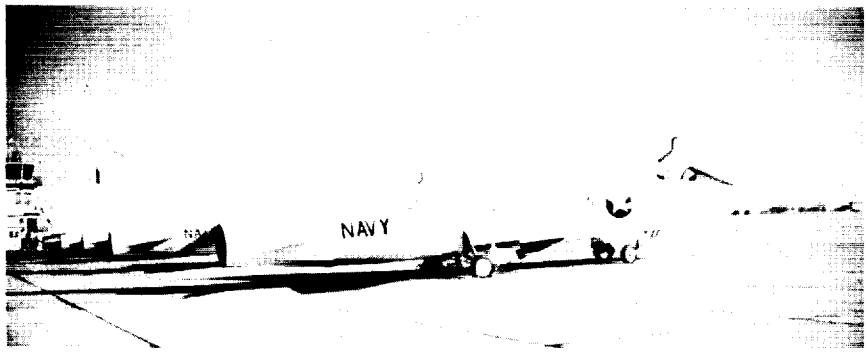

(a) Airplane A. L-97110

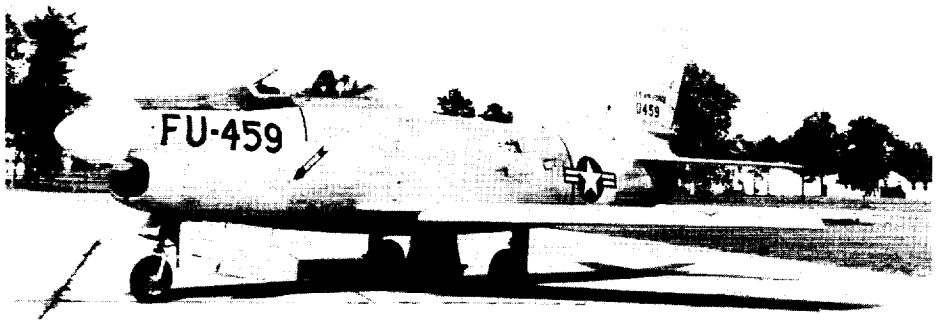

(b) Airplane B. L-89422

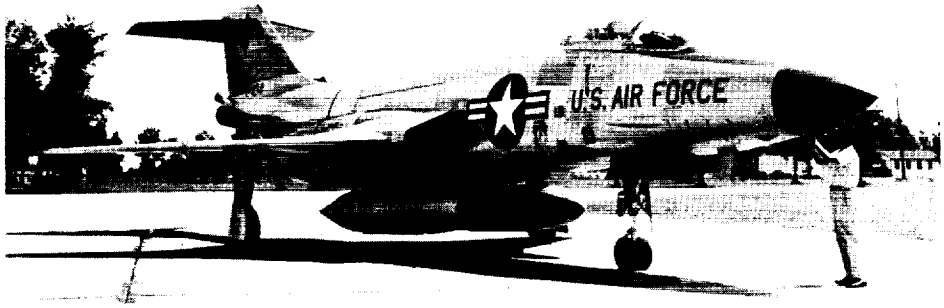

(c) Airplane C. L-95152

Figure 2.- Photographs of airplanes.

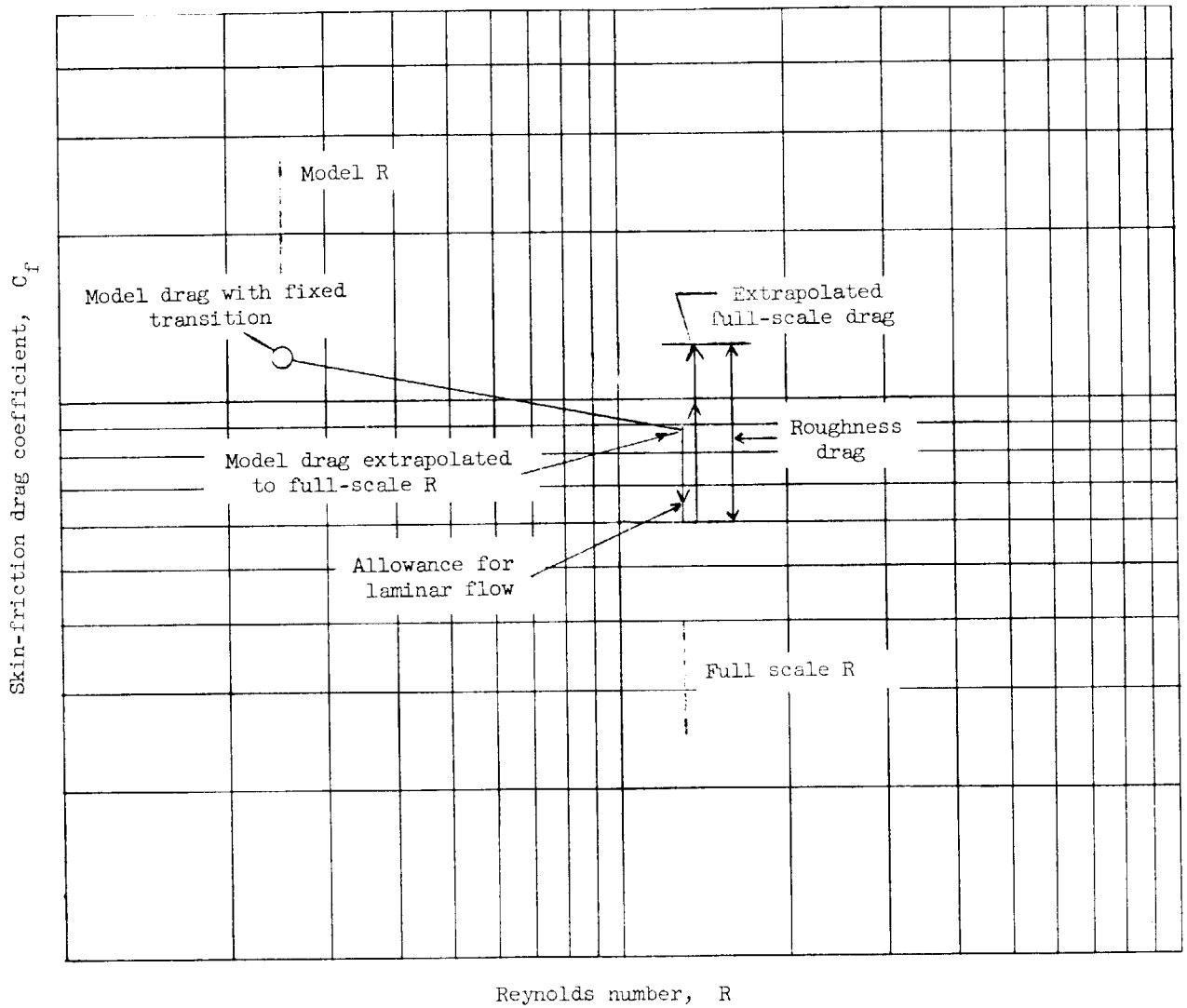

Figure 3.- Schematic presentation of the proposed method of extrapolating model drag data to full-scale airplane.

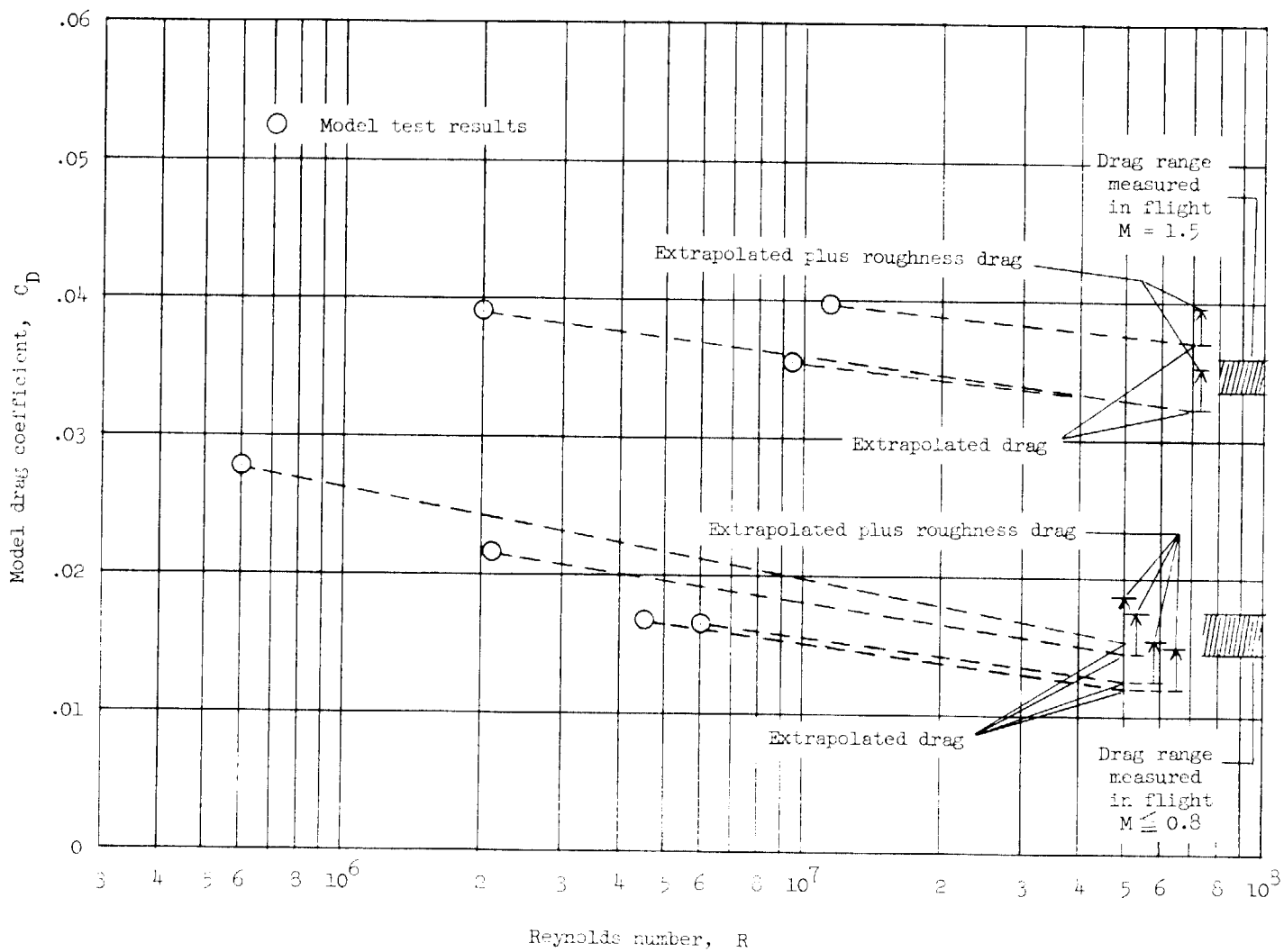

(a) Airplane A.

Figure 4.- Model drag data extrapolated along the turbulent skin-friction curve to full-scale Reynolds numbers plus roughness drag compared with flight drag measurements.

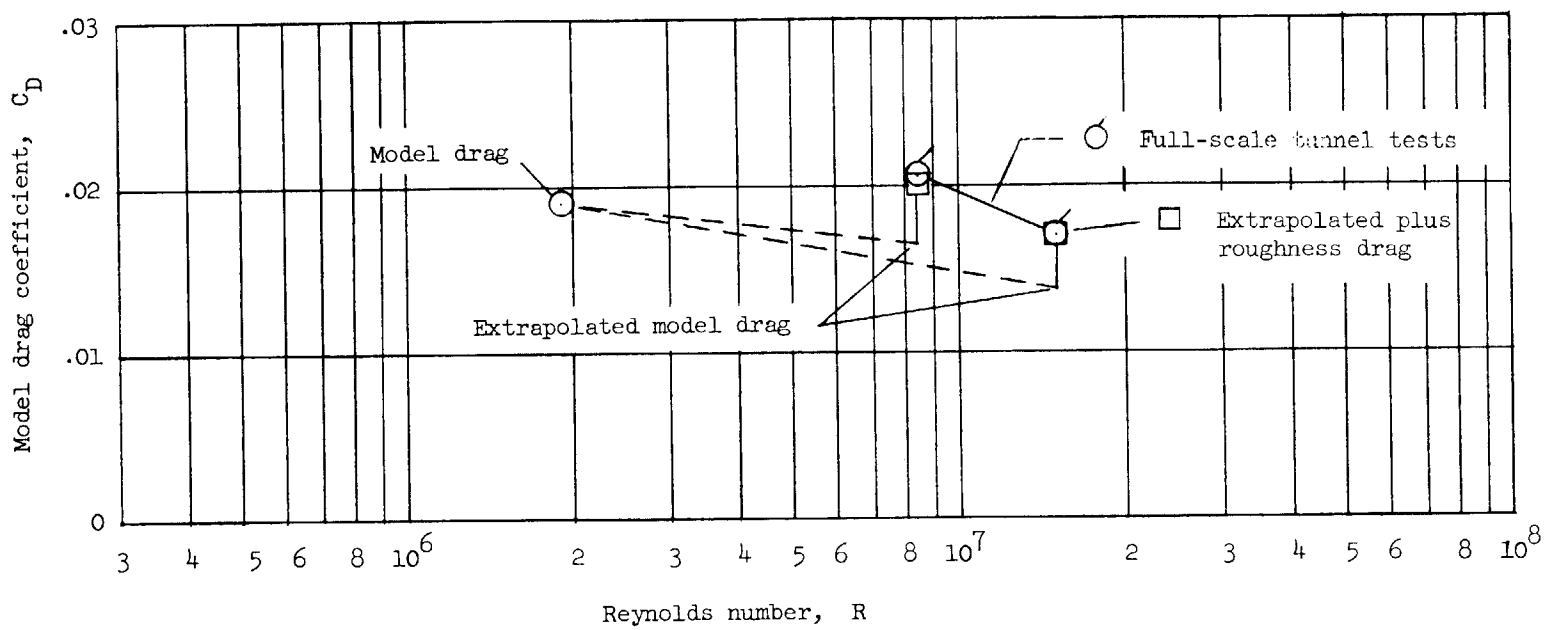

(b) Airplane B.

Figure 4.- Continued.

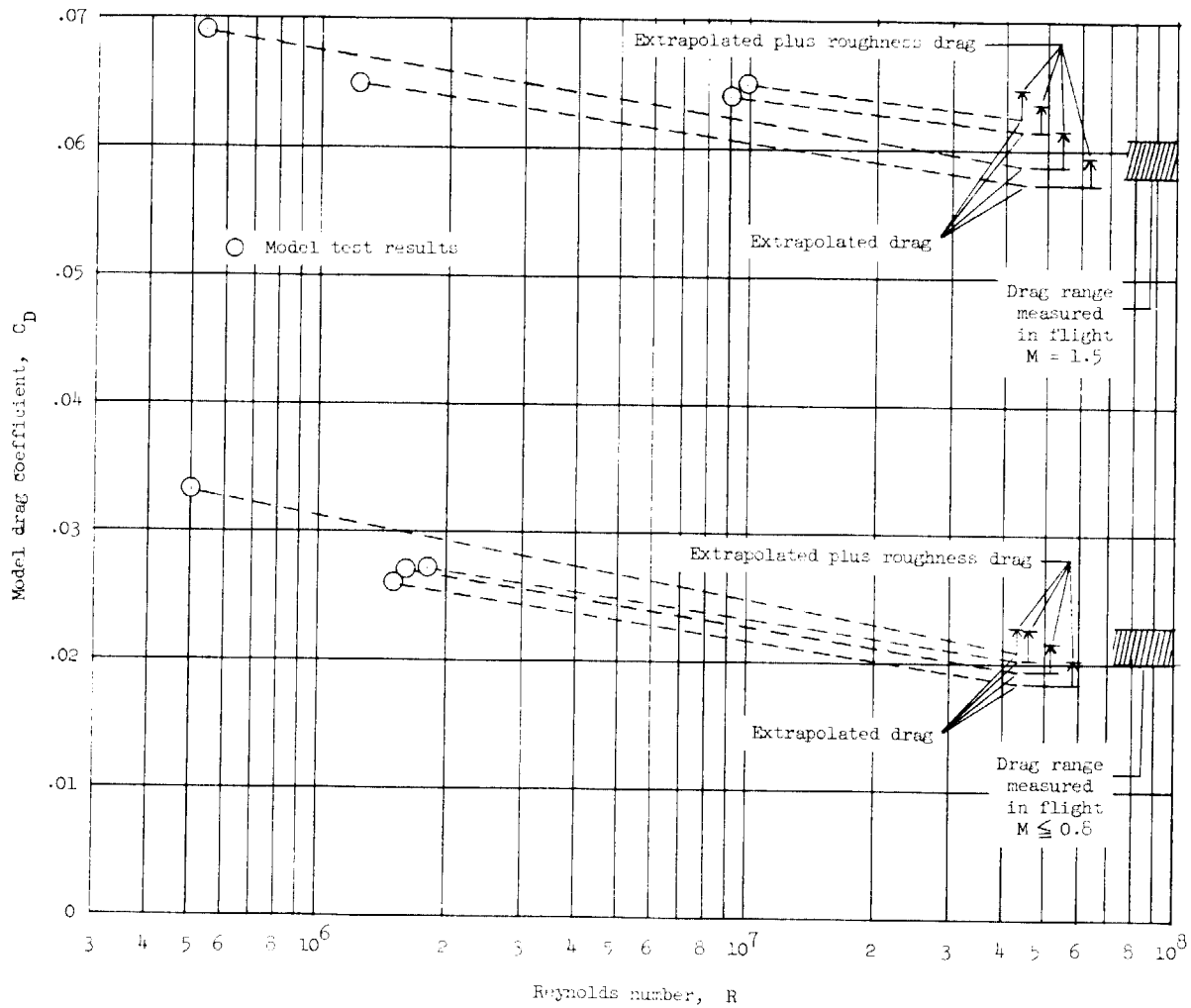

(c) Airplane C.

Figure 4.- Concluded.

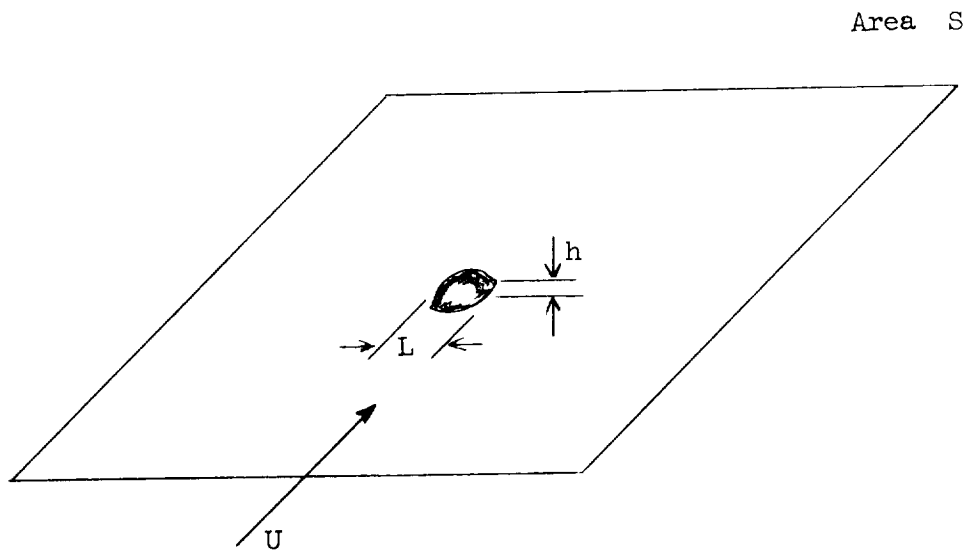

(a) Grain of sand on surface of area S.

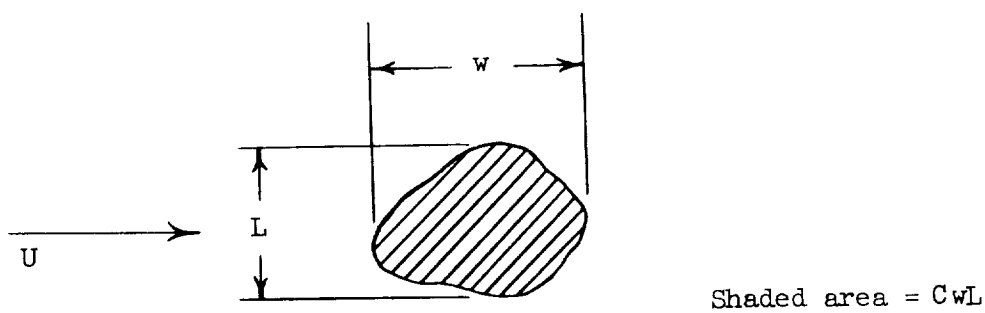

(b) Definition of symbols L, w, C.

Figure 5.- Drawings to show relation of symbols to sand grain.

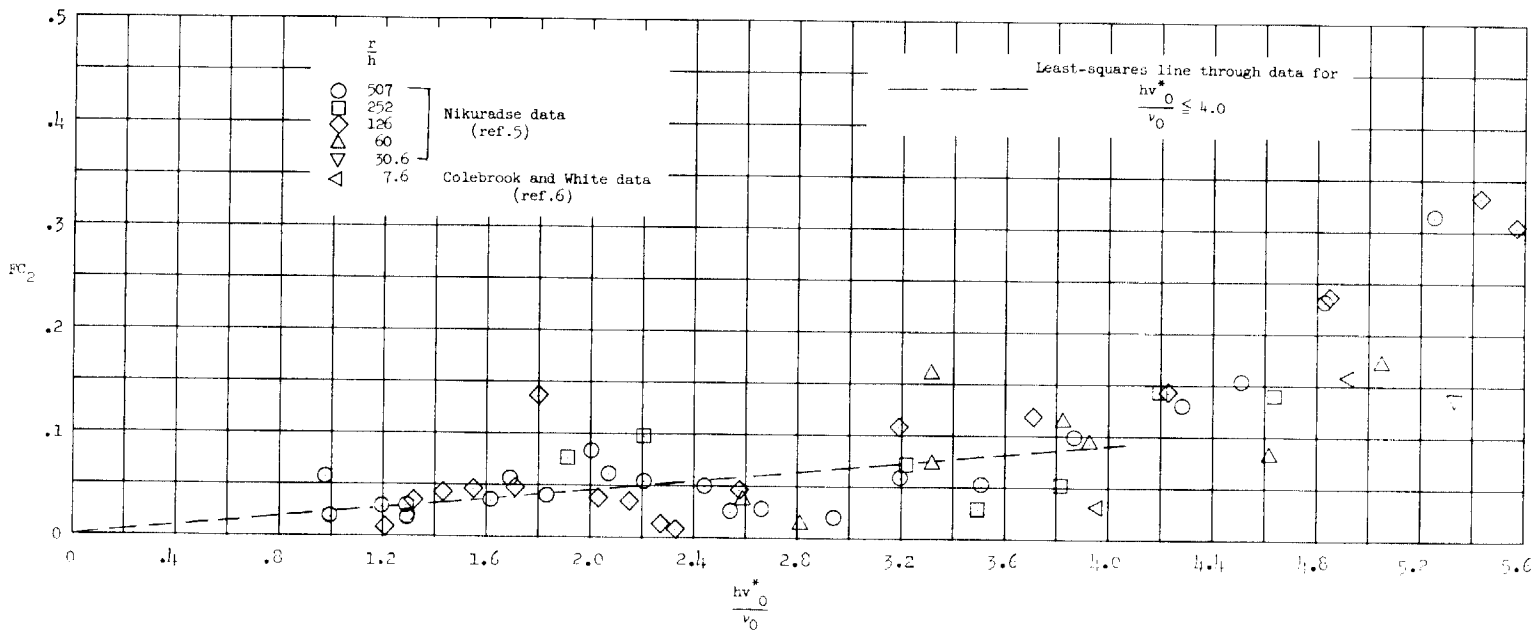

Figure 6.- Calculated values of FC_2 for small values of the roughness parameter $\frac{hv^*_0}{\nu_0}$.

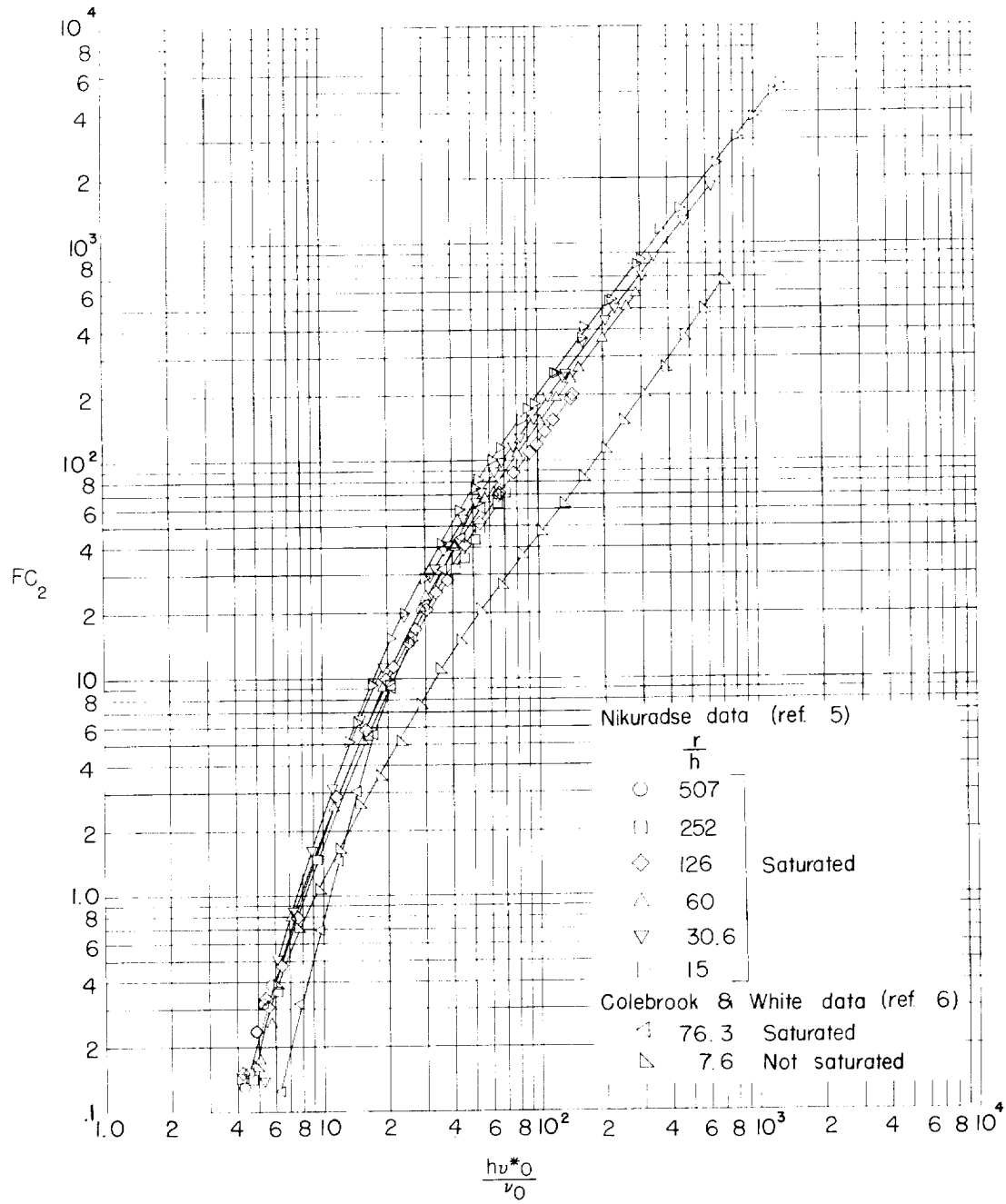

Figure 7.- Calculated variation of FC_2 with $\frac{hv_0^*}{\nu_0}$ for Nikuradse and Colebrook and White sand data.

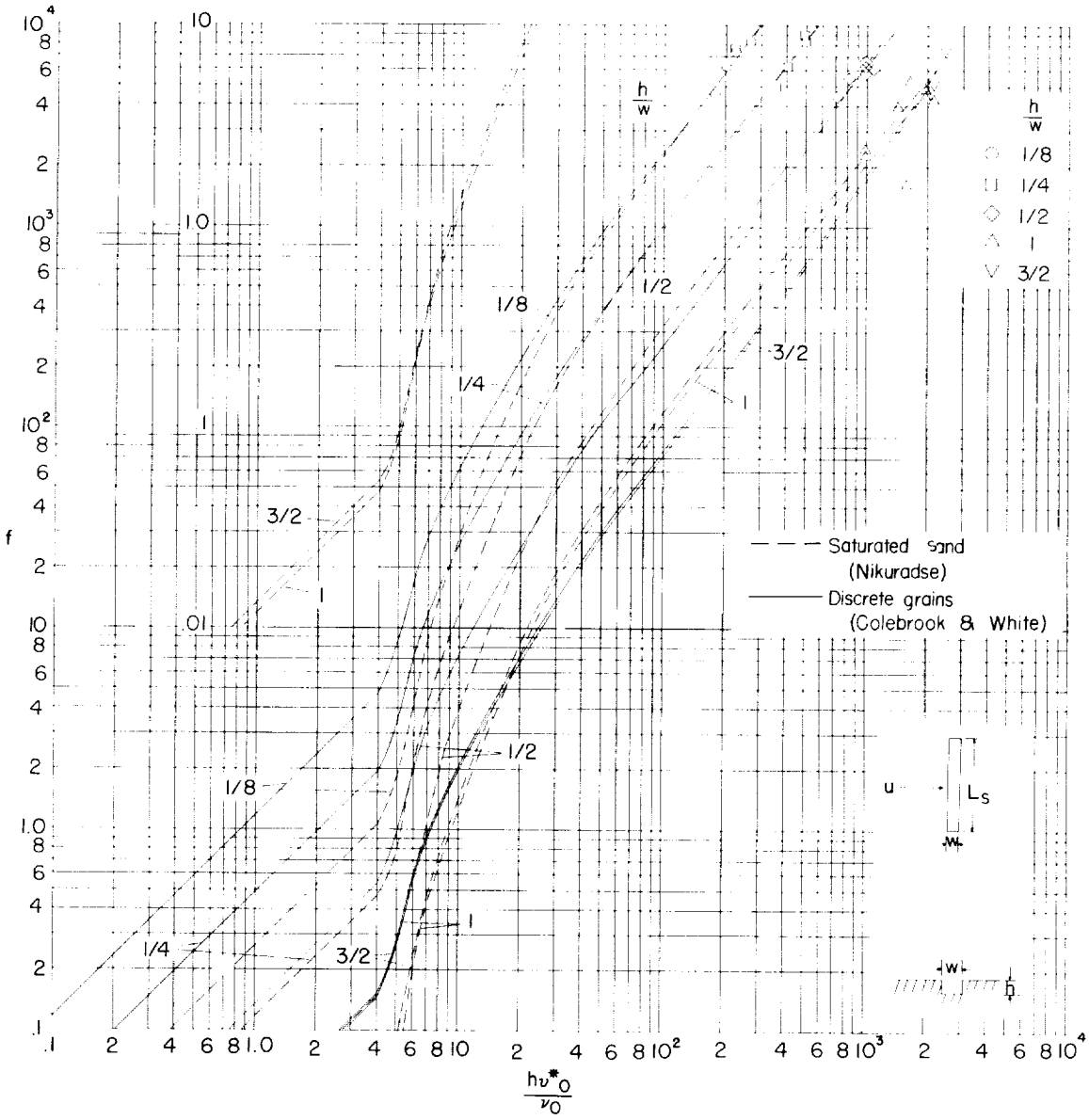

Figure 8.- The f-function for slots or scratches perpendicular to the stream.

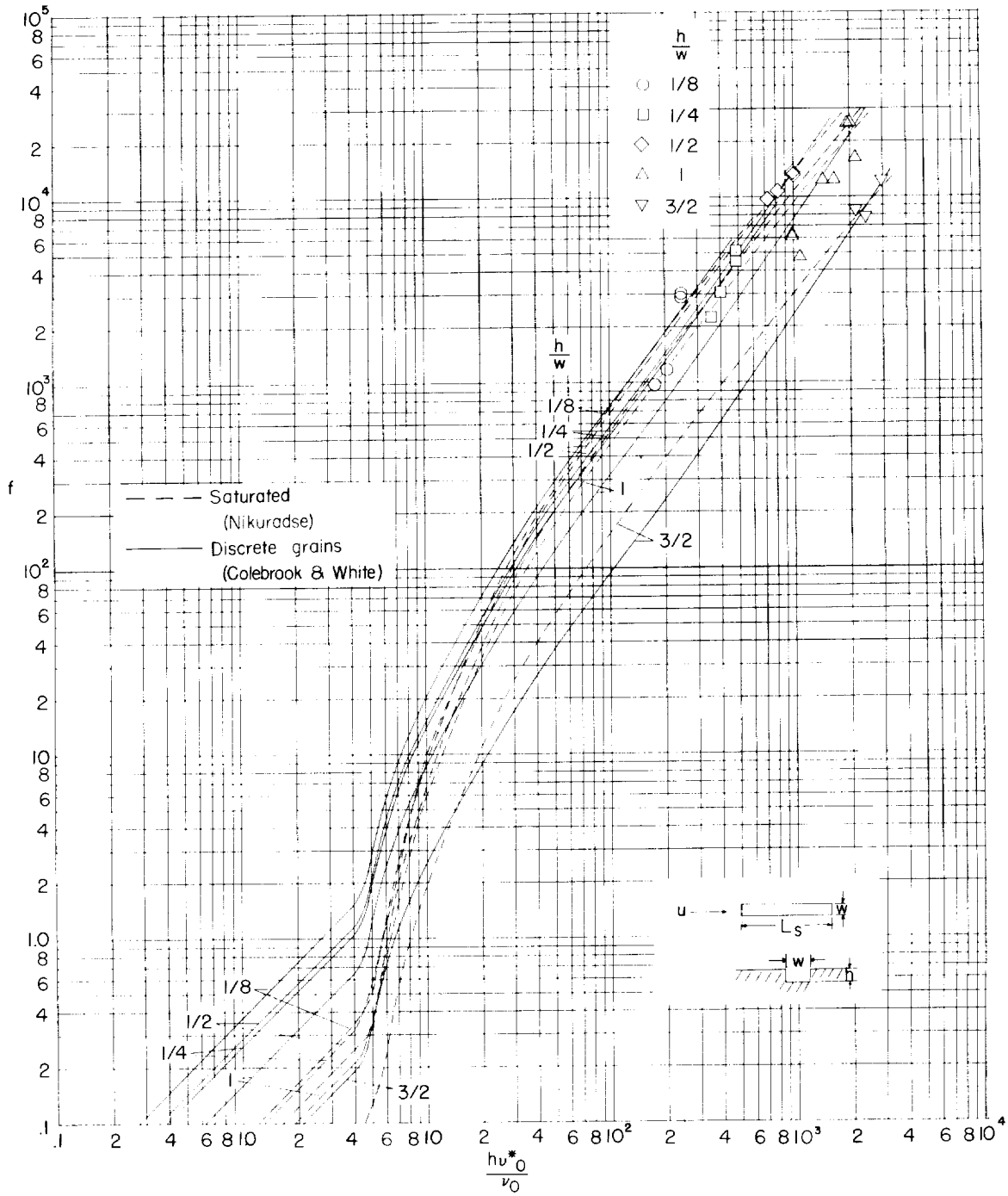

Figure 9.- The f-function for slots or scratches parallel to the stream.

NASA-Langley, 1962 L-295

NASA TN D-1024
National Aeronautics and Space Administration.
MEASURED SURFACE DEFECTS ON TYPICAL TRANSONIC AIRPLANES AND ANALYSIS OF THEIR DRAG CONTRIBUTION. Elmer A. Horton and Neal Tetervin. October 1962. 49p. OTS price, $1.25. (NASA TECHNICAL NOTE D-1024)

Measurements have been made of the surface defects existing on three different operational airplanes. Estimates of the drag increments associated with each type of surface irregularity and comparisons of drags measured on models and the full-scale aircraft indicate that the total drag contribution of the defects is an important percentage of the total airplane drag. Presented in an appendix is an analytical development of a method for estimating the drag contribution of surface scratches that are small in width and depth relative to the boundary-layer thickness.

I. Horton, Elmer A.
II. Tetervin, Neal
III. NASA TN D-1024

(Initial NASA distribution: 1, Aerodynamics, aircraft; 3, Aircraft.)

NASA

NASA TN D-1024
National Aeronautics and Space Administration.
MEASURED SURFACE DEFECTS ON TYPICAL TRANSONIC AIRPLANES AND ANALYSIS OF THEIR DRAG CONTRIBUTION. Elmer A. Horton and Neal Tetervin. October 1962. 49p. OTS price, $1.25. (NASA TECHNICAL NOTE D-1024)

Measurements have been made of the surface defects existing on three different operational airplanes. Estimates of the drag increments associated with each type of surface irregularity and comparisons of drags measured on models and the full-scale aircraft indicate that the total drag contribution of the defects is an important percentage of the total airplane drag. Presented in an appendix is an analytical development of a method for estimating the drag contribution of surface scratches that are small in width and depth relative to the boundary-layer thickness.

I. Horton, Elmer A.
II. Tetervin, Neal
III. NASA TN D-1024

(Initial NASA distribution: 1, Aerodynamics, aircraft; 3, Aircraft.)

NASA

NASA TN D-1024
National Aeronautics and Space Administration.
MEASURED SURFACE DEFECTS ON TYPICAL TRANSONIC AIRPLANES AND ANALYSIS OF THEIR DRAG CONTRIBUTION. Elmer A. Horton and Neal Tetervin. October 1962. 49p. OTS price, $1.25. (NASA TECHNICAL NOTE D-1024)

Measurements have been made of the surface defects existing on three different operational airplanes. Estimates of the drag increments associated with each type of surface irregularity and comparisons of drags measured on models and the full-scale aircraft indicate that the total drag contribution of the defects is an important percentage of the total airplane drag. Presented in an appendix is an analytical development of a method for estimating the drag contribution of surface scratches that are small in width and depth relative to the boundary-layer thickness.

I. Horton, Elmer A.
II. Tetervin, Neal
III. NASA TN D-1024

(Initial NASA distribution: 1, Aerodynamics, aircraft; 3, Aircraft.)

NASA

NASA TN D-1024
National Aeronautics and Space Administration.
MEASURED SURFACE DEFECTS ON TYPICAL TRANSONIC AIRPLANES AND ANALYSIS OF THEIR DRAG CONTRIBUTION. Elmer A. Horton and Neal Tetervin. October 1962. 49p. OTS price, $1.25. (NASA TECHNICAL NOTE D-1024)

Measurements have been made of the surface defects existing on three different operational airplanes. Estimates of the drag increments associated with each type of surface irregularity and comparisons of drags measured on models and the full-scale aircraft indicate that the total drag contribution of the defects is an important percentage of the total airplane drag. Presented in an appendix is an analytical development of a method for estimating the drag contribution of surface scratches that are small in width and depth relative to the boundary-layer thickness.

I. Horton, Elmer A.
II. Tetervin, Neal
III. NASA TN D-1024

(Initial NASA distribution: 1, Aerodynamics, aircraft; 3, Aircraft.)

NASA